UNIVERSIDADE DE LISBOA
FACULDADE DE CIÊNCIAS
DEPARTAMENTO DE BIOLOGIA VEGETAL

Plasmodium berghei/SARS-CoV-2 co-infection phenotype in murine models

Ana Catarina Freire Fraga

Mestrado em Biologia Molecular e Genética

Dissertação orientada por:
Miguel Prudêncio, PhD
Rita Zilhão, PhD

2022

Acknowledgements

Antes de mais, queria agradecer-te a ti, **Miguel**, pela oportunidade de ingressar no teu laboratório e começar esta aventura rodeada de pessoas que, sem dúvida, constituem uma equipa extraordinária. Obrigada pelo voto de confiança para iniciar este projeto e me dares a liberdade de o explorar de uma forma curiosa e criativa, por me teres acompanhado e incentivado nos momentos de euforia, mas também por me teres motivado naqueles em que me senti mais frustrada. Acima de tudo, obrigada pela amizade e por teres proporcionado um ambiente no qual fui capaz de aprender e crescer. És e continuarás a ser uma inspiração para mim e para todos os que te rodeiam.

Andreia, como deves imaginar, será difícil sintetizar aqui o que significas para mim e o quão importante foste durante todo este percurso, tanto profissional como pessoalmente. O teu apoio incondicional, a tua amizade e a nossa "simbiose", como o Miguel tão eloquentemente colocaria, foram fundamentais ao meu progresso durante este ano. Obrigada por todo o acompanhamento e orientação, por todas as brincadeiras, todas as gargalhadas e todos os momentos partilhados, que faziam o trabalho não parecer trabalho. Nunca me deixaste desmotivar e sempre me incentivaste a sonhar mais alto. És, sem dúvida, uma pessoa de referência para mim e para todos, pela tua dedicação e rigor ao executar qualquer tarefa, disponibilidade para ajudar o próximo e pelo carinho com que acolhes todos os que entram na tua vida. Levarei tudo isto comigo, sempre.

Aos restantes membros do laboratório, devo também um grande agradecimento. A ti, **Helena**, por todo o apoio durante o desenvolvimento deste projeto, mas também pela eterna boa disposição e que alegrou as horas infindáveis passadas no BSL3. Também a ti, **Raquel**, pela disponibilidade constante, tanto para os momentos sérios em que me orientaste e formaste, como para os momentos de diversão. **Carla**, um enorme obrigada por todo a preocupação com todas nós, pela tua incontestável competência e acima de tudo pelo sorriso que sempre trazes contigo. Obrigada também à **Adriana Temporão** que, apesar de já não estar no laboratório, foi muito importante à minha integração no grupo e formação inicial, e à **Diana Fontinha** por se ter mostrado sempre disponível para aconselhar e orientar nesta reta final. Por fim, às minhas companheiras de todas as horas **Diana M.**, **Catarina**, **Rita** e a nossa "prudenciana" honorária, **Marta**, devo-vos um enorme agradecimento por tudo o resto, que não é pouco: amizade, companheirismo, felicidade, cumplicidade, mas também todo o apoio nos momentos mais difíceis. Vocês tornaram todas as manhãs, tardes e eventuais noites uma diversão constante. Igualmente, **Sofia**, apesar de estares connosco há pouco tempo, rapidamente te tornaste numa pessoa importante para todos pela tua personalidade contagiante e boa disposição.

Quero também agradecer a todos os membros do **Luísa Figueiredo Lab**, **Maria Mota Lab** e **Gonçalo Bernardes Lab** que, de uma forma ou de outra, me apoiaram e contribuíram para a concretização deste projeto.

Gostaria também de agradecer ao **Prof. Dr. Francisco Dionísio** por me ter aceitado no mestrado e, por isso, ter permitido que tudo isto se materializasse, e à **Profª. Drª. Rita Zilhão**, por todo o acompanhamento durante este percurso, pelo apoio e constante disponibilidade para me esclarecer e auxiliar.

Um grande obrigado à minha **família**, em particular aos meus **pais**, que sempre me incentivaram a seguir os meus sonhos, me apoiaram incondicionalmente e deram a total liberdade para criar o meu próprio caminho. Aos meus **amigos**, obrigada por me acompanharem neste percurso e o terem tornado tão rico, com um especial obrigado ao **Tiggis,** que sempre tomou tão bem conta de mim.

Dani, a ti deixo-te para o fim porque és a pessoa a quem mais devo. Não encontro as palavras que permitam fielmente expressar a importância que tens para mim e o contributo que tiveste para a pessoa que sou hoje. Contigo conheci um mundo diferente, mais completo e rico, recheado de pessoas e experiências insubstituíveis. Por isto, e aliado ao facto de muitas vezes acreditares mais em mim do que eu própria, sou agora capaz de vislumbrar um futuro que outrora me pareceu inalcançável. Obrigada pela pessoa que és, para mim e para toda a gente que nos rodeia. Nunca duvides do teu valor e do que conseguirás alcançar. Tens muito para oferecer.

"Living a minimally acceptable ethical life involves using a substantial part of our spare resources to make the world a better place."

Peter Singer

Abstract

Coronavirus disease 2019 (COVID-19) and malaria, caused by severe acute respiratory syndrome coronavirus 2 (SARS-CoV-2) and *Plasmodium* parasites, respectively, share geographical distribution, in regions where the latter disease is endemic. Because of this geographic overlap, co-infection cases have emerged, albeit with variable clinical presentations, ranging from faster clinical recovery to worse health outcomes. Given the current epidemiologic status of both diseases, the occurrence of co-infections between SARS-CoV-2 and *Plasmodium* is likely to persist. Thus far, epidemiologic studies and case reports have yielded insufficient data on the reciprocal impact of the two pathogens on either infection and related diseases. As such, an experimental approach of this co-infection is critical for the understanding of how these pathogens interact with each other and the impact of this interaction on the progression of either disease. We established a unique and innovative co-infection model to address this issue experimentally for the first time, employing either transgenic mice expressing SARS-CoV-2's human receptor for cell invasion – the human angiotensin-converting enzyme 2 (hACE2) – or wild-type mice in combination with human- and mouse-infective variants of SARS-CoV-2, respectively, and the rodent malaria parasite, *P. berghei*. Our results demonstrate for the first time that an ongoing SARS-CoV-2 infection impacts the outcomes of a subsequent *Plasmodium* infection. Our data shows that a primary infection by a viral variant that causes a severe disease phenotype leads to an exacerbated anti-viral immune response that markedly impairs a subsequent liver infection by the malaria parasite. Additionally, we demonstrate that a primary infection by a viral variant that causes an attenuated disease phenotype reduces malaria severity in mice subsequently infected with *P. berghei*, partially protecting these animals from experimental cerebral malaria and increasing their survival. Our results have unveiled a hitherto unknown virus-parasite interaction that could have important epidemiological and clinical repercussions in malaria-endemic regions, particularly regarding the management and control of the diseases caused by both pathogens. This work paves the way for the development of other models of co-infection between *Plasmodium* and respiratory viruses in relevant *in vivo* models of disease and we anticipate that it will serve as a steppingstone for further research on co-infections, thus filling an important knowledge gap regarding complex disease presentations.

Keywords: Malaria, COVID-19, co-infection, *Plasmodium*, SARS-CoV-2

Resumo

A malária é uma doença infeciosa responsável por elevada mortalidade em países de baixo rendimento, estando entre as 10 principais causas de morte nestas regiões. Estima-se que, apenas em 2021, tenham ocorrido mais de 200 milhões de casos de malária, 95% dos quais na Região Africana da Organização Mundial da Saúde (OMS), resultando em mais de 600 mil mortes. A malária pode ter diferentes apresentações clínicas, variando de assintomática a severa, sendo a malária não complicada, com sintomas inespecíficos semelhantes aos da gripe, a apresentação mais comum. Porém, pacientes com malária complicada podem desenvolver diversos sintomas severos, entre os quais se inclui a malária cerebral. Esta doença devastadora é causada pela infeção com parasitas intracelulares do género *Plasmodium*, sendo transmitida ao seu hospedeiro intermediário (mamífero, reptil e aviário) por mosquitos *Anopheles* fêmea. Os esporozoítos *Plasmodium* são injetados na pele do hospedeiro durante a picada do mosquito e migram atá ao fígado, onde infetam hepatócitos e passam por uma fase de replicação extensa. Esta fase hepática da infeção, embora obrigatória, é clinicamente silenciosa e culmina com a libertação de milhares de merozoítos de *Plasmodium* na corrente sanguínea, onde ciclicamente invadem eritrócitos, dentro dos quais se multiplicam até levar à sua rutura, causando os sintomas da malária. Também durante esta fase sanguínea da infeção são geradas formas sexuadas do parasita que podem ser subsequentemente ingeridas por um mosquito, no qual são gerados novos esporozoítos, assim completando o ciclo do parasita.

A doença do coronavírus 2019 (COVID-19) espalhou-se rapidamente pelo mundo, dando início a uma pandemia global que, desde o seu aparecimento em 2019, conduziu já a mais de 600 milhões de casos e 6 milhões de mortes globalmente. Os pacientes de COVID-19 podem desenvolver uma grande variedade de sintomas. Embora alguns permaneçam assintomáticos, a maioria desenvolve doença leve a moderada, com sintomas gerais semelhantes aos da gripe. No entanto, em casos severos, os doentes desenvolvem uma resposta imune exacerbada e sistémica, causando danos a vários órgãos, com possível falência multiorgânica e morte. Esta doença é causada pelo vírus *severe acute respiratory syndrome coronavirus 2* (SARS-CoV-2), sendo principalmente transmitida entre hospedeiros via aerossóis. Uma vez dentro do hospedeiro, o SARS-CoV-2 entra nas suas células-alvo através de uma interação específica entre a proteína S (*Spike*) viral e recetores na superfície destas células, sendo a enzima conversora da angiotensina 2 (*angiotensin-converting enzyme 2* ou ACE2) o mais importante desses recetores. Após a entrada na célula, o vírus sequestra a maquinaria celular para seu próprio proveito, culminando na formação de novas partículas virais e na sua saída por exocitose, propagando a infeção.

Coinfeção é definido como infeção concomitante de um hospedeiro ou célula por múltiplas espécies de patogéneos. Este tipo de infeção permite novas interações entre agentes patogénicos e o hospedeiro, podendo culminar em apresentações clínicas de doença inusitadas e com importantes consequências para a saúde humana. A disseminação global da COVID-19 levou a uma sobreposição geográfica entre o SARS-CoV-2 e o *Plasmodium* em regiões endémicas de malária, permitindo o aparecimento de casos de coinfeção com apresentações variáveis, desde recuperações aceleradas a piores resultados de saúde. Perante uma infeção viral, o sistema imunitário do hospedeiro desencadeia um conjunto de respostas inflamatórias antimicrobianas, as quais são também estimuladas durante as etapas iniciais da infeção por parasitas *Plasmodium*. Desta forma colocámos a hipótese de que a resposta imunitária desencadeada por uma infeção SARS-CoV-2, sendo mais ou menos exacerbada consoante a variante viral em questão, poderia afetar a capacidade do *Plasmodium* estabelecer uma infeção subsequente ou, alternativamente, influenciar a sua progressão natural e doença associada. De forma a abordar esta questão, estabelecemos um conjunto de modelos *in vivo* de coinfeção entre SARS-CoV-2 e *Plasmodium*, os quais permitem, pela primeira vez, abordar a coinfeção entre estes dois agentes de uma forma rigorosa e devidamente controlada. Esta abordagem permite ultrapassar algumas das

limitações inerentes aos estudos epidemiológicos em humanos, especificamente a sua incapacidade de abordar patologia de uma forma desprovida de fatores confundidores, tais como comorbilidades e infeções múltiplas, bem como informar sobre a sequência de eventos que levam ao seu desenvolvimento.

Num primeiro modelo, ratinhos transgénicos que expressam a ACE2 humana – o principal modelo usado em estudos pré-clínicos de infeção por SARS-CoV-2 – foram primariamente infetados com uma variante ancestral de SARS-CoV-2 (AnSCV2) e, em diferentes momentos, com esporozoítos do parasita da malária de roedores, *P. berghei*. Os nossos resultados relevaram que a infeção secundária com os parasitas da malária em nada alterou a progressão natural da doença causada pelo AnSCV2 tanto em termos dos sinais clínicos de doença como da replicação viral nos pulmões, quantificada por ensaio de formação de placas virais em células Vero CCL-81. Pelo contrário, a análise de expressão génica do parasita por transcrição reversa e PCR quantitativo (RT-qPCR) revelou que a exposição primária à infeção viral causou uma redução significativa na infeção hepática por *P. berghei*. Ademais, demonstrámos, por microscopia de imunofluorescência, que esta redução decorre especificamente da redução do número de hepatócitos infetados, sem impacto no desenvolvimento intra-hepatocítico do parasita, indicando que a exposição ao AnSCV2 impediu a infeção inicial ou mediou uma rápida eliminação de células infetadas. Tendo em conta estes resultados, e sabendo que a infeção por AnSCV2 induz caracteristicamente um estado de hiperativação imunológica não restrita ao local primário de infeção, procurámos caracterizar os eventos inflamatórios estabelecidos durante a coinfeção, tanto ao nível sistémico como ao nível hepático. Nesse sentido, uma análise histopatológica dos fígados revelou que nenhum dos grupos experimentais de animais apresentava alterações à arquitetura hepática normal, indicando que a diminuição no número de hepatócitos infetados com o parasita não pode ser atribuída a dano hepático inespecífico ou infiltração imune exacerbada induzida pelo AnSCV2. No entanto, a análise de baços por citometria de fluxo multi-paramétrica revelou que, a nível sistémico, a exposição ao AnSCV2 induziu um perfil de resposta imune diferente do observado para os animais infetados apenas com o parasita, observando-se em particular um aumento significativo na ativação de células T adaptativas e no seu recrutamento para a periferia.

Tendo observado que uma infeção primária por AnSCV2 teve um efeito inibitório na fase hepática da infeção pelo por *P. berghei*, procurámos investigar se um efeito semelhante ocorreria durante a fase sanguínea da infeção, independentemente de eventos pré-hepáticos e hepáticos. Nesse sentido, a fase hepática do ciclo de vida do parasita foi contornada através da inoculação direta de eritrócitos infetados com *P. berghei* um dia antes da infeção por AnSCV2. Os nossos resultados demonstraram que os animais coinfetados exibem um fenótipo da doença aparentemente agravado, sem que tenham sido observadas diferenças na replicação viral ou parasitária, avaliadas respetivamente por ensaio de formação de placas virais em células Vero CCL-81 e bioluminescência no sangue. No entanto, este modelo apresenta algumas limitações, nomeadamente no que diz respeito à sua plausabilidade clínica.

Desta forma, e com o intuito de estabelecer um modelo de infeção viral mais atenuado e, portanto, mais clinicamente relevante, foi estabelecido um modelo alternativo de infeção viral baseado numa variante de SARS-CoV-2 adaptada a ratinhos (*mouse adapted SARS-CoV-2 virus strain 10* ou MA10). Contrariamente à AnSCV2, esta variante causa uma infeção não letal, permitindo, assim, uma monitorização total e adequada da patologia associada à malária em ratinhos coinfetados. Dessa forma, ratinhos de estirpe selvagem foram primariamente infetados com a variante MA10 e subsequentemente inoculados com diferentes doses de esporozoítos de *P. berghei*. Embora a exposição ao MA10 não tenha afetado a infeção hepática por *P. berghei*, o seu impacto no resultado da doença durante a fase sanguínea foi claro. Os nossos resultados mostraram que a coinfeção conferiu proteção parcial contra sintomas neurológicos graves e aumentou a sobrevivência, quando comparado com ratinhos apenas infetados com o parasita. Interessantemente, esses efeitos foram independentes de qualquer atraso na patência ou alteração da capacidade replicativa do parasita no sangue, sugerindo que o fenótipo de proteção possa ser mediado por alterações nos eventos inflamatórios que levam a patologia severa em malária.

Este trabalho abordou experimentalmente, pela primeira vez, o impacto de uma infeção por SARS-CoV-2 no estabelecimento e progressão de uma infeção subsequente por *Plasmodium* em modelos *in vivo* relevantes. Os nossos resultados permitiram desvendar um conjunto de interações entre um vírus respiratório e um parasita que eram até então desconhecidas. Dada a atual situação epidemiológica da malária, coinfeções entre *Plasmodium* e outros patógenos, incluindo vírus respiratórios, continuarão a ocorrer. Assim, o nosso trabalho abre caminho ao desenvolvimento de modelos adicionais de coinfeção entre vírus respiratórios e parasitas da malária que permitam elucidar a forma como cada um modula e influencia as respostas do hospedeiro a infeções pelo segundo. Tal permitirá colmatar uma importante lacuna de conhecimento relativamente a apresentações decorrentes de doenças complexas e respetivos desfechos.

Palavras-chave: Malária, COVID-19, coinfeção, *Plasmodium*, SARS-CoV-2

Table of Contents

Index of Figures

Index of Tables

Abbreviations

ACE2: Angiotensin-converting enzyme 2

ACK: Ammonium-chloride-potassium lysis buffer

AIDS: Acquired immunodeficiency syndrome

AnSCV2: European ancestral strain of SARS-CoV-2

APC: Antigen presenting cell

ARDS: Acute respiratory distress syndrome

BSL3: Biosafety level 3

cDNA: Complementary deoxyribonucleic acid

CMC: Carboxymethyl cellulose

COVID-19: Coronavirus disease 2019

DAMP: Damage-associated molecular pattern

DC: Dendritic cell

DGAV: Direção-Geral da Alimentação e Veterinária

DMEM: Dulbecco's modified Eagle's medium

DNA: Deoxyribonucleic Acid

dpi: Days post infection

ECM: Experimental cerebral malaria

EEF: Exoerythrocytic form

FELASA: Federation of European Laboratory Animal Science Associations

FSC: Forward-scatter

FVD: Fixable viability dye

GFP: Green fluorescent protein

hACE2: Human angiotensin-converting enzyme 2

HI-FBS: Heat inactivated-foetal bovine serum

HIV: Human immunodeficiency virus

Hprt: Hypoxanthine guanine phosphoribosyl transferase

IFN: Interferon

IL: Interleukin

IMM JLA: Instituto de Medicina Molecular João Lobo Antunes

I.n.: Intranasal

I.p.: Intraperitoneal

iRBCs: infected Red Blood Cells

I.v.: Intravenous

K18-hACE2 C57BL/6: Transgenic C57BL/6 mice that constitutively expresses the hACE2 under the human keratin 18 promoter

MA10: mouse adapted SARS-CoV-2 virus strain 10

MERS: Middle East respiratory syndrome

MERS-CoV: Middle east respiratory syndrome coronavirus

NK: Natural killer cell

NKT: Natural killer T cell

PAMP: Pathogen-associated molecular pattern

***Pb*GFP-Luc$_{con}$:** Transgenic *Plasmodium berghei* ANKA that constitutively expresses GFP-luciferase fusion

PBS: Phosphate-buffered saline

PCR: Polymerase chain reaction

PFU: Plaque-forming units

PPR: Pattern recognition receptor

PV: Parasitophorous vacuole

qPCR: Quantitative PCR

RBC: Red blood cell

RLU: Relative luminescence units

RNA: Ribonucleic acid

rRNA: Ribosomal ribonucleic acid

RPMI: Roswell Park Memorial Institute

RT-qPCR: Reverse transcription quantitative PCR

RT: Room temperature

SARS: Severe acute respiratory syndrome

SARS-CoV: Severe acute respiratory syndrome coronavirus

SARS-CoV-2: Severe acute respiratory syndrome coronavirus 2

SD: Standard deviation

SPF: Specific-pathogen-free

spz: Sporozoite

SSC: Side-scatter

T_N: Naïve T cell

T_{CM}: Central memory T cell

T_{EM}: Effector/effector memory T cell

TCR: T cell receptor

TMPRSS2: Transmembrane serine protease 2

UIS4: Upregulated in infective sporozoites 4

Vero CCL-81: *Verda reno* cell line from African green monkey (*Chlorocebus sabaeus*)'s kidney from ATCC® (CCL-81™)

WHO: World Health Organization

1. INTRODUCTION

1.1. Malaria

Etiology, transmission and symptoms

Malaria is an infectious mosquito-borne disease caused by intracellular protozoan parasites of the *Plasmodium* genus.[1] Malaria parasites have one definitive insect host (female *Anopheles* mosquitoes) and one intermediate host, which may be one of various vertebrate species, including mammals, reptiles and birds.[1,2] Although more than one hundred *Plasmodium* species have been identified, only four of them use humans as an almost exclusive natural intermediate host, namely: (i) *P. falciparum*, the most prevalent species in the World Health Organization (WHO) African Region, responsible for the more severe forms of the disease and the highest malaria-related mortality; (ii) *P. vivax*, the most globally widespread species, corresponding to 2% of total malaria cases, with a high prevalence in the densely populated WHO Regions of Southeast Asia and Western Pacific, and being the predominant species in the WHO Region of the Americas; (iii) *P. ovale*, a rare species mostly found in West Africa, responsible for a mild clinical presentation; and (iv) *P. malariae*, also rare but, if left untreated, capable of causing chronic infection with severe consequences, such as nephrotic syndrome.[1-3] Overall, *P. falciparum* and *P. vivax* pose the greatest threat to human health, accounting for the majority of cases.[1] Moreover, *P. knowlesi*, a simian (*Macaca* spp. genus) malaria parasite, has also been periodically and increasingly reported to infect humans, especially in Southeast Asia.[1,4]

Malaria can have different clinical presentations, depending on the *Plasmodium* species, parasitaemia levels and the host's immune status.[1,5] Generally, malaria is curable if promptly diagnosed and treated. Otherwise, it can lead to severe complications and even death.[1] Three main degrees of disease severity can occur, specifically: (i) asymptomatic malaria, in which parasites can be detected but do not lead to clinical signs, occurring mainly in malaria-endemic areas where years of repeated exposure induce partial immunity; (ii) uncomplicated malaria, the most common clinical presentation; and (iii) complicated/severe malaria.[1] The clinical manifestations of uncomplicated malaria are mainly non-specific flu-like symptoms, such as fever, chills, sweats, headaches and myalgias that tend to appear 10 to 15 days after the bite of an infected mosquito. However, this incubation period may vary from 7 to 30 days, depending on parasite species.[1] In turn, complicated malaria is associated with severe organ failures and/or abnormalities in metabolic and blood parameters, with symptoms varying according to age group: children more frequently present neurologic abnormalities (loss of consciousness, seizures and behaviour alterations, known as cerebral malaria), severe anaemia, metabolic acidosis and acute respiratory distress syndrome (ARDS), while acute kidney and liver injury are more frequent in adults, with neurologic and acidosis symptoms still being moderately frequent.[1,6] Overall, although *P. falciparum* infections are the most likely to progress to severe malaria, *P. vivax* and *P. malariae* can also lead to splenomegaly and nephrotic syndrome, respectively.[1] Interestingly, infections by *P. vivax* and *P. ovale* have the particular ability to establish dormant liver-stage parasite forms (known as hypnozoites), which may reactivate months or years after the first infection and symptom clearance, causing disease relapses with an important impact on health outcomes.[1,7,8]

The life cycle of *Plasmodium* spp.

The bite of an infected female *Anopheles* mosquito deposits an average of 15-123 motile sporozoites – the mosquito salivary gland-resident forms of the parasite – into the dermis of the mammalian host (**Figure 1.1**).[9] A portion of the injected *Plasmodium* sporozoites enter the bloodstream and reach the liver, where they traverse multiple hepatocytes before productively invading one, with formation of a parasitophorous vacuole (PV).[10,11] During a period of 2 to 16 days, depending on the *Plasmodium* species, the parasite multiplies inside the PV, a phase known as the liver- or hepatic-stage

of infection.[1,9] In a process termed hepatic schizogony, these exoerythrocytic forms (EEFs) produce thousands of blood-infective parasite forms, known as merozoites, which are subsequently released into circulation enveloped in vesicles derived from host cell membranes, called merosomes, inside which the parasite is able to pass undetected through the liver-resident macrophages (Kupffer cells).[12] As mentioned above, *P. vivax* and *P. ovale* can also establish a liver latency period by forming non-replicating EEFs (hypnozoites), which prolong parasite survival and may lead to clinical relapses. Following merosome burst, the released merozoites invade red blood cells (RBCs) inside which the parasite undergoes consecutive rounds of asexual replication, known as erythrocytic schizogony. This process culminates in the production of multiple daughter merozoites and in the subsequent burst of the infected RBC, restarting the blood stage cycle every 24 to 72 h, depending on the *Plasmodium* species.[1,13] This phase is termed the blood- or erythrocytic-stage of *Plasmodium* infection. The type of RBCs infected also depends on the *Plasmodium* species: *P. vivax* exclusively infects reticulocytes, leading to lower levels of parasitaemia, whilst *P. falciparum* is not restricted to one cell type, leading to higher levels of parasitaemia and a more severe infection.[1,13] Whilst the liver stage of the parasite's life cycle is obligatory but clinically silent, the blood stage of infection is entirely responsible for the symptoms of malaria. Also during the blood stage of infection, some merozoites differentiate into sexual forms of the parasite, termed the male and female gametocytes, which remain in the bloodstream for several days, thus increasing the probability of being ingested by a female *Anopheles* mosquito during a blood meal.[13] Once ingested by a mosquito, the environmental conditions inside its midgut induce gametocyte maturation into gametes, which then fuse to produce diploid zygotes.[1] The latter become motile and elongated ookinetes that penetrate the midgut wall and give rise to oocysts. Oocysts grow by asexual replication and eventually rupture, releasing thousands of sporozoites that migrate to the mosquito's salivary glands. The cycle is resumed when the mosquito takes a blood meal from a new mammalian host, inoculating sporozoites into the skin.

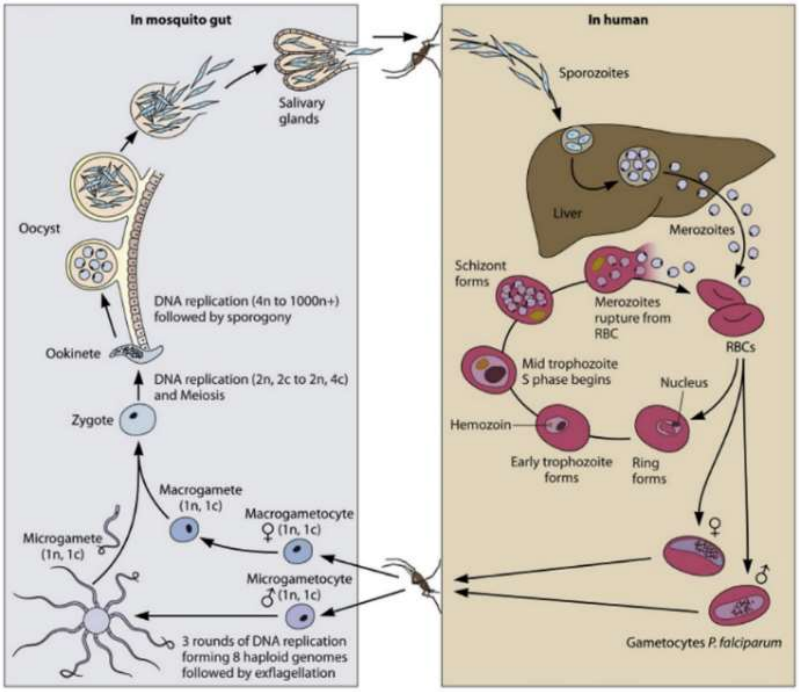

Figure 1.1 - Life cycle of *Plasmodium*.[14] The bite of an infected female *Anopheles* mosquito deposits sporozoites into the mammalian host's skin, which will migrate toward the liver and individually infect hepatocytes. The liver-stage development produces merosomes containing multiple merozoites that are released into the blood stream, infecting red blood cells. Inside these cells, asexual replication occurs, perpetuating the infection inside the mammalian host. Moreover, some blood-stage parasites undergo sexual differentiation, giving rise to gametocytes that are ingested by uninfected mosquitoes during a blood meal. Inside the mosquito's midgut, gametocytes undergo sexual replication, producing sporozoites that migrate and establish themselves in the salivary glands, renewing the infection cycle.

1.2. COVID-19

Etiology, transmission and symptoms

Coronavirus disease 2019 (COVID-19) is a viral disease caused by the severe acute respiratory syndrome coronavirus 2 (SARS-CoV-2), a virus that rapidly spread globally, giving rise to a global pandemic, as declared by the WHO on 11 March 2020.[15,16] SARS-CoV-2 is a positive-sense single-stranded RNA virus of the Nidovirales order, belonging to the *Coronaviridae* family and *Betacoronavirus* genus.[17,18] This family of viruses has some distinctive characteristics, specifically: (i) it possesses the largest and most complex known viral RNA genomes, with a total size ranging from 28 to 31 kb, protected by association with a nucleocapsid protein; (ii) the genome encodes a proof-reading enzyme besides the usual RNA polymerase, allowing lower mutation rates; and (iii) it possessed a studded envelope, consisting of Spike/S protein trimers, forming a crown-like structure that gave rise to the name *corona* (Latin for crown).[17] These coronaviruses have vertebrates as exclusive hosts (mammal and avian species), and spread between individuals by direct contact, aerosols and the fecal-oral route, or through contact with contaminated surfaces.[17] Interestingly, these viruses have a particular tendency to cross species barriers, i.e. to transit from their natural host species to a different one.[19]

Several coronaviruses are responsible for respiratory infections in humans, ranging from seasonal upper respiratory infections, such as the "common cold", to more severe forms, such as severe acute respiratory syndrome (SARS), Middle East respiratory syndrome (MERS) and, more recently, COVID-19.[17,18] Traditionally, the development of more severe respiratory diseases, gastroenteritis and encephalitis in humans were rare events and the common infections did not appear to induce long-lasting immunity. However, in 2002 and 2013, previously uncharacterized coronaviruses appeared in Southeast Asia and the Middle East, respectively.[20,21] These pathogens, later termed SARS coronavirus (SARS-CoV) and MERS coronavirus (MERS-CoV), had zoonotic origins but could also infect humans, causing severe disease and ultimately death. SARS-CoV human-to-human transmission was mainly driven by small droplets of saliva or trough contact with infected surfaces, leading to rapid disease spread across several countries, with more than 8000 reported cases and an overall case fatality of 10%.[18] As for MERS-CoV, camels were the major reservoir host but simultaneously served as infection vehicles to humans, with human-to-human transmission being improbable. Nonetheless, it was responsible for more than 2500 cases, with an overall case fatality of 35%.[18] These two outbreaks alerted the world to the existence of zoonotic coronaviruses that could also have a severe impact on human health. More recently, in 2019, China faced the emergence of a novel coronavirus, SARS-CoV-2, that, similarly to others, seemed to have a zoonotic origin, even though the animal reservoir has not yet been identified.[22,23]

Patients with COVID-19 may develop a large array of clinical manifestations, which arise after an incubation period between 2 and 19 days, depending on the viral variant, patient age group and presentation severity.[24] These clinical manifestations can range from general (fever, fatigue) to system-specific symptoms, including respiratory, gastrointestinal, urinary tract, musculoskeletal, cardiovascular and neurological, with the particular presentation varying according to disease severity and duration (acute *versus* long COVID-19).[25] While some patients remain asymptomatic, most develop mild to moderate disease, presenting mainly general flu-like symptoms. However, patients that develop more severe forms of the disease suffer from aggravated respiratory tract symptoms with specific organ deterioration – such as SARS – , and may enter a systemic inflammatory state, generally associated with a cytokine storm which can lead to multiorgan failure and possibly death.[26,27] Poor prognosis has been associated with various risk factors, including age above 65 years, tobacco consumption, diabetes, cardiovascular disease, chronic lung disease, malignancy and immunosuppression.[28]

SARS-CoV-2 infection cycle

SARS-CoV-2 transmission occurs mainly through the formation of aerosols that are projected or remain suspended in the air during coughing, sneezing, or even normal breathing and speaking of an infected patient.[22,29] These particles can directly infect another individual in close contact, mainly through the respiratory tract by inhalation, but also by direct particle contact with the eyes, nose and mouth.[22,29]

Once inside the organism, SARS-CoV-2 enters its target cells via receptor-mediated membrane fusion or endocytosis (**Figure 1.2**).[18] This interaction is mediated by the binding of the virus' S protein to host cell receptors, specifically angiotensin-converting enzyme 2 (ACE2) and transmembrane serine protease 2 (TMPRSS2), the latter being responsible for cleavage and subsequent activation of the S protein, thus allowing membrane fusion and viral entry.[30,31] TMPRSS2 acts synergistically with the Furin protease, which is responsible for pre-cleavage of the S protein at a different site during viral exit from the cell. However, this step is neither sufficient nor an absolute requirement for infection.[30,32,33] Naturally, the tissue distribution and binding affinity of these proteins significantly condition overall viral tropism and pathology: ACE2, TMPRSS2 and Furin, the dominant players in SARS-CoV-2 infection, are highly enriched in respiratory and gastrointestinal tract tissues, pancreas, kidney gallbladder and, interestingly, in the placenta. However, given the more restricted expression of ACE2, it constitutes the limiting factor for successful viral infection within a tissue.[19,34,35]

After successful cell invasion, the virus hijacks the host cell's machinery to translate its genomic RNA into proteins responsible for the subsequent synthesis of full-length copies of the viral genome. This allows further production of viral components that are encapsulated in newly formed viral particles, which finally exit the cell by exocytosis.[17,18] During this process intermediate molecules, such as double-stranded RNAs, are produced and can be recognised as pathogen-associated molecular patterns (PAMPs) by the host cells, triggering innate antimicrobial immune responses.[36] However, it has been hypothesized that this detection is partially averted by the formation of perinuclear double-membrane vesicles inside of which viral genome replication is conducted, thus creating a microenvironment that allows protection from the cytosolic PAMP recognition receptors and subsequent evasion from innate immune responses.[18] Another process by which coronaviruses are thought to modulate the host's immune responses to infection is the translation of accessory proteins encoded in the viral genome. These proteins can vary between virus species and their function is largely unknown. However, some are thought to have interferon antagonism or immune evasion properties that will determine viral pathogenicity.[17,18]

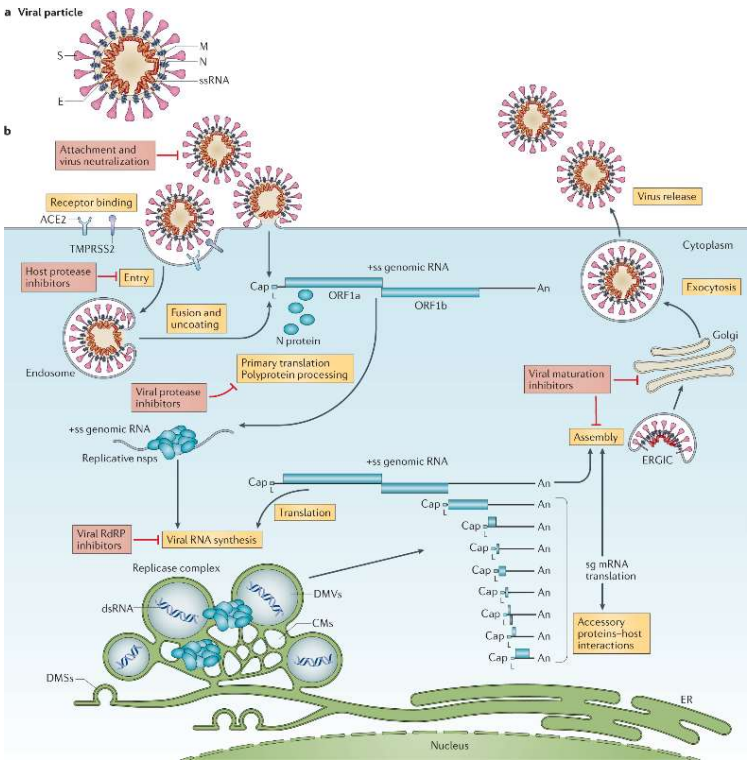

Figure 1.2 – SARS-CoV-2 virion structure and replicative cycle.[18] **(A)** The virion consists of positive-sense single-stranded RNA (+ssRNA) encapsulated by the nucleocapsid (N) protein and an envelope (E) containing the membrane (M) and spike (S) proteins. **(B)** The virus attaches to cellular factors, such as Angiotensin-converting enzyme 2 (ACE2) and transmembrane serine

protease 2 (TMPRSS2) through S protein interactions, promoting viral uptake and fusion with host cell membranes. Inside the cell, uncoating and release of the genetic material occurs, allowing translation by host machinery. The resulting non-structural proteins (nsps) will then participate in viral genome replication and transcription inside perinuclear vesicles. Structural proteins are produced and translocated through the endoplasmic reticulum (ER) and ER-to-Golgi intermediate compartment (ERGIC) where they interact with newly produced genomic RNA culminating in particle budding into the cell lumen and exocytosis. DMVs, double-membrane vesicles; CMs, convoluted membranes; DMSs, double-membrane spherules; Sg mRNA, subgenomic messenger RNAs; cap, 5′ cap structure; L, leader sequence; ORF, open reading frames; An, 3′ polyAdenilated sequence; RdRP, RNA-dependent RNA polymerase, dsRNA, double-stranded RNA.

1.3. Socio-economic burden of Malaria and COVID-19

According to the WHO, malaria remains a major public health problem, constituting one of the top 10 causes of death in low-income countries, along with five other infectious diseases.[37] Malaria is transmitted in tropical and subtropical areas where temperature and humidity conditions favour the survival and multiplication of the *Anopheles* mosquitoes, thus allowing the completion of the parasite's growth cycle inside the vector.[1] According to WHO's most recent report, in 2021, the 84 malaria-endemic countries were affected by 247 million cases, 95% of which occurred in the WHO African Region, followed by 2% in South-East Asia.[3] This disease burden resulted in an estimated 619 thousand deaths globally, mainly in children aged under 5 years old, who account for 77% of total malaria deaths. Like in 2020, both cases and deaths showed an increase compared with the data from 2019, being mainly attributed to service disruption during the COVID-19 pandemic.[3] However, despite all the efforts to achieve malaria eradication, the decrease in malaria incidence and mortality had already been slowing down since 2015.[3] In addition to its major health toll, malaria also carries a heavy individual and governmental economic burden, both related to prevention and treatment costs, but also indirect costs associated to illness, such as absenteeism from work or school, loss of productivity, among others. These conditions greatly limit the economic growth of these countries, perpetuating a vicious cycle of poverty and poor health outcomes.[38,39]

Since its emergence in 2019, COVID-19 has posed an unquestionable socio-economic and health burden globally. According to the WHO, as of 14th December 2022, more than 640 million cases have been confirmed and 6 million deaths reported.[40] Moreover, besides the major direct health impact illustrated by these numbers, this disease has also overwhelmed the global health system, resulting in a significant increase in overall mortality by various infectious and non-infectious diseases.[41] Additionally, the specific prevention measures undertaken during the pandemic, specifically the generalized lockdowns, had major economic consequences worldwide, even in countries with a low incidence of infection. This drastic change in the global economy resulted in an equally dramatic social impact, involving loss of income and jobs, increased poverty, less access to education, and food insecurity, amongst others.[42]

Ultimately, these two infections represent major public health problems and their co-existence in malaria-endemic countries has already been shown to have major impact on malaria control and prevention. However, infection with both pathogens may also have other unpredictable epidemiologic and clinical consequences that can greatly impact the efficacious management of both infections and, subsequently, the socio-economic recovery in these countries.

1.4. Co-infections

Co-infection is defined as the concurrent infection of a host or single cell by multiple pathogen species. This type of infection is particularly important in human health since it enables new interactions between the co-infecting agents to occur within the host, possibly giving rise to unexpected phenotypes.[43] In the case of malaria, numerous studies have already demonstrated interactions between *Plasmodium* and other infectious agents, either from other species, specifically bacteria, viruses and other parasites, or from the same species, the latter being known as *Plasmodium* superinfections.[44] These interactions may aggravate[45-48] or, conversely, decrease[49-52] the pathogenicity of one or both agents.

This section will address not only some of the most epidemiologically relevant co-infections involving *Plasmodium*, specifically with Human immunodeficiency virus (HIV) and *Mycobacterium tuberculosis*, but also with Influenza virus, which may provide clues about possible interactions between malaria parasites and SARS-CoV-2.

HIV-acquired immunodeficiency syndrome (HIV-AIDS) is the last stage of an HIV infection, where marked immunosuppression is present and the host becomes more susceptible to opportunistic infections, including by *Plasmodium*.[53] Alongside malaria and tuberculosis, HIV-AIDS is one of the top 10 causes of death in low-income countries, with the WHO African Region being the most affected (25.4 million estimated cases in 2020), followed by the Americas and South-East Asia (both with an estimated 3.7 million cases in 2020).[37] Given their clinical and epidemiological relevance, *Plasmodium*/HIV co-infections have been extensively studied. These studies indicate that: (i) *Plasmodium* induces an increase in HIV viral load and CD4+ T cell depletion, which in turn leads to further immunosuppression and disease aggravation;[54,55] and (ii) HIV reciprocally increases susceptibility to *Plasmodium* infection;[47,56,57] making this co-infection an example of mutual aggravation.

Tuberculosis is an airborne bacterial disease caused by *M. tuberculosis*, that constitutes another major public health problem, being responsible for an estimated 10 million new cases in 2020, most of which in the South-East Asia (43%), Africa (25%) and Western Pacific (18%) WHO regions.[58] In some African countries, simultaneous *M. tuberculosis* and *Plasmodium* infection have been reported with significant prevalence[59,60] and some studies have shown important immune modulation in co-infected hosts[61-63]. These interactions resulted in either malaria-induced aggravation of tuberculosis[45,64] or tuberculosis-induced inhibition of malaria, although the latter remains controversial[50,64,65].

Viruses that cause respiratory tract infections, such as Influenza viruses, also have a high prevalence in malaria-endemic countries[66,67] and cases of co-infection with *Plasmodium* have been reported[68,69]. Interestingly, some of the studies regarding this co-infection seem to indicate that an Influenza virus infection reduces the likelihood of acquiring a concomitant *Plasmodium* infection.[70-72] Regarding SARS-CoV-2, its geographic overlap with *Plasmodium* is evident (**Figure 1.3**) and co-infection cases have been reported, albeit with variable clinical presentations, ranging from faster clinical recovery to worse health outcomes.[73-81] Nevertheless, collective analysis of co-infection case reports suggests that co-infected patients have lower laboratory alterations than patients infected only with SARS-CoV-2.[82] In addition, some observational studies suggested an interaction leaning toward protection from poor health outcomes in SARS-CoV-2/*Plasmodium* co-infected patients in malaria-endemic countries, as mortality due to COVID-19 was found to negatively correlate with malaria prevalence.[83,84] In accordance, another study showed that previous high exposure to *P. falciparum* appears to lead to a lower proportion of severe or critical COVID-19 cases than low exposure.[85] Nonetheless, none of these studies are able to fully clarify the possible interactions occurring between SARS-CoV-2 and *Plasmodium*, and its consequences for either infection and disease progression.

A

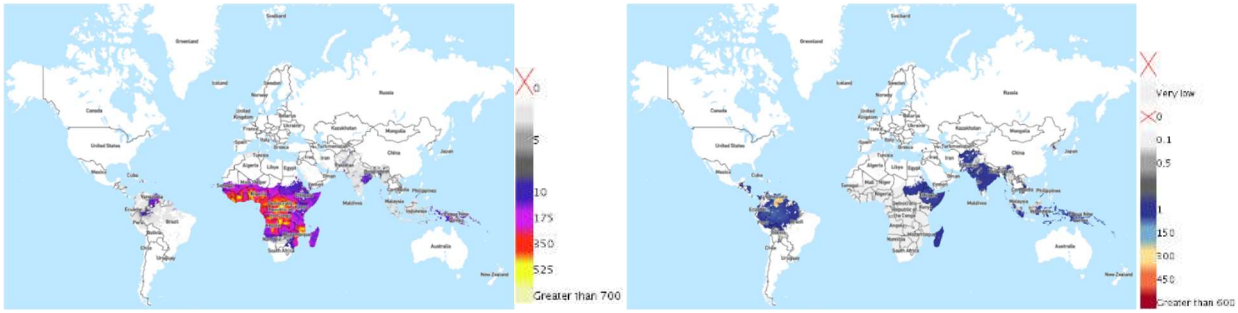

B

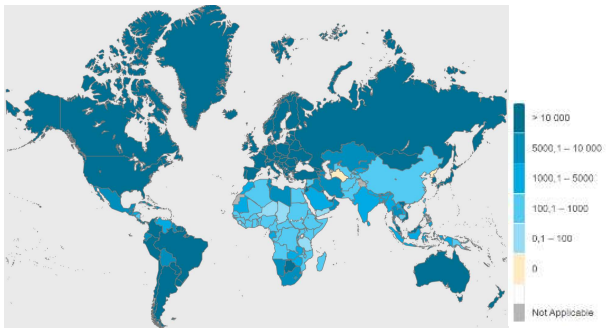

Figure 1.3 – Health burden of malaria and COVID-19. (A) *P. falciparum* (on the left) and *P. vivax* (on the right) malaria cases per 1.000 population at risk, 2000-2019 (*World Health Organization Collaborating Centre in Geospatial Disease Modelling. The Malaria Atlas Project*).[86] **(B)** COVID-19 cases per 100.000 population, 2022 (*WHO Coronavirus COVID-19 Dashboard. Published 2022. Accessed December 14, 2022. https://covid19.who.int/*).[40]

1.5. Experimental models for malaria and COVID-19

Although humans would constitute the ideal system to study complex disease processes, obvious ethical reasons restrict their participation in scientific research to epidemiological, genetic and clinical studies or to post-mortem analysis. Whilst still informative, these approaches have limited scientific utility in unveiling the sequential events that lead to pathology and doing so in a way that is devoid of confounding factors, such as comorbidities and multiple co-infections.[87,88] Alternatively, despite the debate around their ability to truthfully replicate human pathology, the usefulness of animal models for research purposes, particularly mice, is unquestionable. Indeed, mouse models allow the study of complex diseases, molecular mechanisms and several other biologically relevant processes and phenomena in a whole-organism context, in a fairly reproducible way.[87] In addition, the development of efficient methods for genetic manipulation of mice enabled the creation of unique experimental conditions otherwise impossible to simulate.[89,90] A good example of this are humanized mouse models in which mice engrafted with human genetic material or human tissues (organs, tumors, complete immune system, microbiome, *etc*) can be used for rigorous and comprehensive study of complex human processes.[91,92]

For COVID-19 research, the ability of inserting human genetic material in mice, specifically the receptor for SARS-CoV-2 viral entry into human host cells – the human ACE2 (hACE2) – , was pivotal in the global response to the pandemic. These humanized mice have shown to present physiological changes consistent with those observed in COVID-19 patients, including hematologic alterations, humoral and cellular responses (interstitial pneumonia, extra-pulmonary pathology and cytokine profile alterations), thus being extensively used as SARS-CoV-2 infection models. This in turn enabled fast development of a plethora of vaccines candidates and therapeutics, whilst also serving as important models for basic research on SARS-CoV-2 pathogenicity and immunopathology.[93-96] Moreover, being generated in long established and well-studied mouse genetic backgrounds, these

humanized models arise as promising candidates for the study of interactions between SARS-CoV-2 and other infectious agents in the same host.

Regarding malaria research, multiple species of rodent malaria parasites are available, including *P. berghei, P. yoelii, P. chabaudi* and *P. vinkei* [87], and methods for their genetic manipulation have been developed and widely employed.[97] These parasites can be further combined with a variety of mouse models, each combination having certain specificities in terms of parasite biology and infection outcomes (e.g. lethal or nonlethal models). The number of possible mouse-parasite combinations is extensive and enables researchers to focus on different aspects of malaria pathology.[87,98,99] Through these models, a deeper understanding of the players involved in infection, host-parasite interactions and host immune responses can be achieved, thus unveiling their specific contribution to pathology and clinical phenotypes.[98] Taking *P. berghei* ANKA parasites and C57BL/6J mice – a widely employed combination – as an example, this model leads to a neurologic syndrome resembling human cerebral malaria, termed experimental cerebral malaria (ECM).[98,99] This ECM has been associated with molecular mechanisms that mimic those that occur in humans, including inflammation within the brain, breakdown of the blood-brain barrier and migration of parasite-specific CD8+ cytotoxic T cells to the brain. Besides the neurologic pathology, this model also recapitulates many other important aspects of severe malaria in humans, including acute lung pathology and respiratory distress, liver damage, metabolic acidosis, adherence of parasite-infected red blood cells in tissue microvasculature (designated "sequestration") and correlation of total body parasite count with disease severity.[88,100] Furthermore, research-related advantages should be equally recognized since: (i) *P. berghei* is a robust, well-characterized rodent-infecting agent that does not pose a threat to humans;[101] and (ii) C57BL/6J mice are more susceptible to hepatic infection than other mouse strains.[102] Gathering all this evidence, the *P. berghei* ANKA-C57BL/6J mice combination has proved to be an excellent model to study severe malaria and a feasible alternative to human studies.

1.6. Aims

Overall, numerous case reports and observational studies indicate that interactions between SARS-CoV-2 and *Plasmodium* in co-infected patients may impact the clinical progression of disease and pathology. Given the considerable geographical overlap between these infections, understanding how they mutually interact is of major relevance for adequate management of either disease in malaria-endemic regions. Despite their possible impact, the nature of these interactions is not yet understood, nor has it been the subject of experimental study in relevant *in vivo* co-infection models. As such, this project aims to fill this knowledge gap by:

(i) Assessing the reciprocal impact of a *P. berghei*/SARS-CoV-2 co-infection on the progress of the two infections and their associated diseases;

(ii) Establishing relevant *in vivo* co-infection models that may facilitate the identification of the mechanisms that underly any observed co-infection phenotypes.

These goals will be pursued through the establishment of the most suitable host/parasite/virus combinations to obtain relevant *in vivo* co-infection models. State-of-the-art methodologies will be used to assess disease phenotypes, quantify *Plasmodium* and SARS-CoV-2 infection loads, and investigate immune responses to infection.

2. MATERIALS AND METHODS

2.1. Experimental animals

Wild-type C57BL/6J mice purchased from Charles River Laboratories were housed in the specific-pathogen-free (SPF) facilities of Instituto de Medicina Molecular João Lobo Antunes (IMM JLA). Heterozygous K18-hACE2 C57BL/6J mice from The Jackson Laboratory were bred and housed in the same facility. Experimental animals (8-11 weeks old) were handled in biosafety level 3 (BSL-3) conditions and all experimental work involving animals has been reviewed and approved by The Animal Welfare Body of iMM JLA, which is in accordance with the current legislation (Directive 2010/63/Eu and Decreto-lei 113/2013) and follows the Federation of European Laboratory Animal Science Associations (FELASA) guidelines. All procedures are included in the research project "Transgenic hACE2 mice model of SARS-CoV-2 infection", which has already been licensed by the National authority DGAV – Direcção Geral de Alimentação e Veterinária (license number: 001878-2021).

2.2. Parasite lines

Transgenic luciferase-expressing *P. berghei* ANKA rodent malaria parasites, line 676m1cl1, in which the firefly luciferase transgene is fused with green fluorescent protein (GFP) and constitutively expressed under the control of *eef1aα* promoter (*Pb*GFP-Luc$_{con}$, hereafter referred to as *P. berghei*), were kindly provided by Chris Jansen Lab (Leiden University) and employed throughout.[103]

2.3. Viruses

All studies with SARS-CoV-2 viruses were performed in a certified BSL3 laboratory, following international safety guidelines. Two virus strains were employed: (i) an European ancestral strain of SARS-CoV-2 virus (herein referred as AnSCV2) isolated at iMM JLA from a clinical sample (European Nucleotide Archive sample accession SAMEA6844881) and contributed by Dr. Pedro Simas (Católica Medical School); and (ii) a mouse-adapted SARS-CoV-2 virus strain 10 (herein referred as MA10) obtained from the BEI Resources repository (NR-55329) and kindly provided by Dr. Gonçalo Bernardes (IMM JLA). Viral stocks were titrated and stored at -80ºC until further use.

2.4. *In vivo* infections

2.4.1. *P. berghei* liver-stage infection

P. berghei sporozoites were obtained from laboratory-reared infected *A. stephensi* mosquitos. Mosquitoes were infected by feeding on the blood of *P. berghei*-infected mice and salivary glands were extracted by hand dissection 20 to 30 days later and collected into non-supplemented Roswell Park Memorial Institute medium (RPMI, Thermo Fisher Scientific).[104] Free sporozoites were obtained by mechanical homogenization of the salivary glands and subsequent filtration through a 40 µm strainer. Sporozoites were counted in a Neubauer chamber and diluted in non-supplemented RPMI medium to the desired concentration. Experimental mice were infected by retro-orbital intravenous (i.v.) injection of $3x10^4$ sporozoites/200 µL, under isoflurane anaesthesia.[105]

2.4.2. *P. berghei* blood-stage infection

P. berghei-infected red blood cells (iRBCs) were obtained from a donor mouse (passage mouse), infected by intraperitoneal (i.p.) injection of a freshly thawed stock of *P. berghei*-parasitized blood. Five days later, the passage mouse was euthanized and blood was collected by cardiac puncture. The parasitaemia of the collected blood was assessed microscopic examination of Giemsa-stained blood smears and quantification of the iRBCs:Red Blood Cells (RBCs) ratio, and haematocrit was assessed by

counting RBCs in a Neubauer chamber. The *P. berghei*-parasitized blood was diluted in 1x PBS (Merck) to the desired concentration. Experimental mice were infected by i.p. injection of $1x10^6$ iRBCs/200 µL.

2.4.3. SARS-CoV-2 infection

Aliquots of AnSCV2 and MA10 viral stocks were thawed and diluted in 1x PBS to the desired concentration for each experiment. Mice were infected by intranasal (i.n.) inoculation of either a higher dose of $2.5x10^4$ plaque-forming units (PFU)/50 µL or a lower dose of $1x10^4$ PFU/20 µL, under isoflurane anaesthesia.

2.5. Assessment of infection and disease phenotypes

2.5.1. Weight and clinical score

Body weight and clinical signs were monitored daily after the first pathogen infection and until euthanasia. Signs of disease were recorded using a modified version of the clinical score described in [106], with the employed version ranging from 0 to 7 points and evaluated parameters including back arching (0-1 points), ruffled fur (0-2 points), activity (0-3 points) and respiratory difficulties (0-1 points). Euthanasia was performed whenever a 20% decrease in body weight was reached and/or severe signs of disease (total score of 6 or higher) were recorded.

2.5.2. Assessment of liver infection

Livers were collected 46 h[107] after sporozoite inoculation by dissection of mice following euthanasia by isoflurane inhalation. Each liver was divided in three parts for different purposes: (i) the caudate lobe, as well as the superior and inferior right lobes (0.7-0.9 mg of liver sample), were used for quantification of parasite gene expression by reverse transcriptase quantitative polymerase chain reaction (RT-qPCR)[108], using specific primers (see sequence in **Appendix – Supplementary table 1**); (ii) the left liver lobe was fixed and processed for immunofluorescence microscopy analysis; and (iii) the median liver lobe was stored in 4% formaldehyde (Enzifarma) at room temperature (RT) until further analysis.

RNA extraction and RT-qPCR

Mouse liver samples were mechanically homogenized in TRIzol reagent (BioRad, Hercules, CA, USA) using BMT-20-S-M-gamma Tubes (IKA-Werke GmbH & Co.KG) and left 1 h at RT to allow viral inactivation, as a safety measure.[95] The samples were then removed from the BSL-3 facility and stored at -80ºC until further analysis. RNA was extracted following the manufacturer's instructions, purified with ethanol[109] and quantified using NanoDrop DR 2000 Spectrophotometer (Thermo Fisher Scientific). Complementary DNA (cDNA) was synthesized from 1 µg of RNA using the NZYTech cDNA synthesis kit (NZYTech) and random hexamer primers, according to the manufacturer's recommendations and employing the following thermocycling parameters: 25°C for 10 min, 55°C for 30 min, and 85°C for 5 min. cDNA was amplified by quantitative PCR (qPCR) using an Applied Biosystems 7500 Fast Real-Time PCR System, in which each 10 µL reaction contained 5 µM of Power SYBR Green PCR Master Mix (Applied Biosystems, Thermo Fisher Scientific) and 0.5 µM of each primer (forward and reverse) and employing the following thermocycling parameters: 50ºC for 2 min, 95°C for 10 min, 40 cycles at 95ºC for 15 s and 60°C for 1 min with melting stage of 95ºC for 15 s, 60ºC for 1 min and 95ºC for 30 s. DNase treatment was not required as primers were designed to span exon-exon junctions, avoiding genomic DNA amplification.

Melting curve analysis and addition of controls lacking RNA were used to confirm the specificity of amplification and to assess the formation of primer dimers. Gene expression was analysed

by the comparative CT (ΔΔCT) method, using the mouse-housekeeping gene hypoxanthine guanine phosphoribosyl transferase (Hprt) for normalization of the expression level of all genes.

Immunofluorescence microscopy analysis of liver slices

Mouse liver samples were fixed in 4% paraformaldehyde (SantaCruz Biotechnology) overnight at 4-8ºC, sectioned into 50 µm thick slices using a Vibrating blade microtome Leica VT 1200S, stained and analysed using an adapted version of the protocol described in [107]. Briefly, liver slices were incubated in permeabilization/blocking solution containing 2% Albumin Bovine Serum (VWR Chemicals) and 0.5% Triton-X100 (Carl Roth) in 1x PBS for 1 h at RT. The parasite's surrounding membrane was stained with a goat anti-UIS4 primary antibody (1:300 dilution; Siagen) overnight at 4-8ºC, followed by incubation with donkey Alexa Fluor 488 anti-goat antibody (1:500 dilution; Invitrogen, Thermo Fisher Scientific) and Hoechst 33342 double stranded DNA dye (1:1000 dilution; Invitrogen, Thermo Fisher Scientific) for 2 h at RT. Primary and secondary antibodies, as well as DNA dye, were diluted in permeabilization/blocking solution and each antibody incubation was followed by 3 washes with 1x PBS and 5 min agitation. Stained liver slices were mounted on microscope slides with Fluoromount G (Invitrogen, Thermo Fisher Scientific) and image acquisition was carried out using a Zeiss Cell Observer inverted widefield fluorescence microscope. Image processing for number and size quantification of exoerythrocytic parasite forms (EEFs) was performed using Fiji software version 1.53t.

Histopathology

Mouse liver samples were fixed in 4% formaldehyde (Enzifarma), processed overnight (see protocol in **Appendix – Supplementary table 2**) and paraffin (Leica) embedded in a transversal orientation. Stereology-sectioning into ten 3 µm thick slices was carried out using a Minot Microtome Leica RM2145 and slides were stained with hematoxylin (Bio-optica) and eosin (Merck) (see protocol in **Appendix – Supplementary table 2**). Analysis of tissue sections was carried out by Dr. Pedro Faísca from Instituto Gulbenkian Ciência's Histopathology Facility, using a NanoZoomer-SQ Digital slide scanner (Hamamatsu Photonics) and included identification of (i) intracellular parasite forms (EEFs); (ii) hepatocellular damage; and (iii) inflammatory infiltrates.

2.5.3. Assessment of *P. berghei* blood infection

Mouse parasitaemia was quantified daily after injection of *P.berghei*-iRBCs by a bioluminescence assay using a modified version of the protocol described in [110]. Briefly, 5 µL of blood were collected from mice's tail vein into 45 µL of Firefly luciferase lysis buffer (Biotium) at the selected time points and stored at -20 ºC until further analysis. Prior to analysis, the samples were spun down and 15 µL of the mixture was pipetted to a 96-well white plate. Luminescence was determined by adding 50 µL of D-luciferin dissolved in Firefly luciferase assay buffer to each well and immediately measuring luminescence in a Tecan Infinite M200 Plate Reader (Tecan). Values of luciferase activity are expressed as relative luminescence units (RLU)**.**

2.5.4. Assessment of SARS-CoV-2 pulmonary infection

Mouse pulmonary SARS-CoV-2 infection was assessed either 4 or 5 days post viral inoculation and quantified by virus titration by a plaque-forming assay using Vero cells from ATCC® (CCL-81™).

Lungs were collected by dissection of experimental mice following euthanasia by isoflurane inhalation. The left lung was used for quantification of infectious viral particles. After collection, the lung was mechanically homogenized in 3 mL of homogenization medium (see composition in **Appendix – Supplementary table 3**) using BMT-20-S-M-gamma Tubes (IKA-Werke GmbH & Co.KG), and subsequently clarified by centrifugation (300 g for 3 min at RT) and stored at -80ºC until further analysis.

Plaque assay

Adherent Vero CCL-81 cells were cultured and maintained in growth media (composition in **Appendix – Supplementary table 3**) at 37 ºC with 5% CO_2. One day prior to virus titration, cells were seeded into 6-well plates at a density of $8x10^5$ cells/well in growth media. On the day of titration, lung homogenates were ten-fold serially diluted in maintenance medium (see composition in **Appendix – Supplementary table 3**). Growth medium was removed from the cultured cells and 0.5 mL of each viral dilution were added per well. The plates were incubated in a CO_2 incubator for 1 h and gently rocked every 15 min. The inoculum was discarded from each well, 2 mL of overlay medium (medium composition in **Appendix – Supplementary table 3**) was added, and the plates were incubated in a CO_2 incubator for 4 days. The overlay medium was then removed from the cells and cells were fixed with 4% formaldehyde for 1 h and stained with 0.1% toluidine blue for 30 min. Viral plaques were counted using a magnifying glass and the viral titer was calculated as PFU/mL, according to:

$$\text{PFU/mL} = \text{average number of plaques} \times \frac{1}{\text{dilution}} \times \frac{1}{\text{inoculum}}$$

Total viral titers per left lung where then calculated and further normalized to respective lung weight.

2.5.5. Immunophenotyping

Spleens were collected upon euthanasia, mechanically homogenized, and filtered through a 70 μm filter to isolate leukocytes. The samples were then centrifuged (at 500 g for 5 min at RT) and resuspended in 1 mL of Ammonium-Chloride-Potassium (ACK) lysis buffer (see composition in **Appendix – Supplementary table 4**), followed by a 4 min incubation at RT for RBC depletion. The lysis reaction was stopped by addition of 3 mL of FACS buffer (see composition in **Appendix – Supplementary table 4**). The leukocyte suspension was further centrifuged (at 500 g for 5 min at RT) and resuspended in 1 mL of FACS buffer for subsequent surface staining and total live cell counts in an BD Accuri™ C6 Plus Flow Cytometer. One million leukocytes were added to 1.5 mL tubes containing 100 μL of 1x PBS, centrifuged at 500 g for 5 min at RT, and incubated in 15 μL of Fc block (eBiociences, Thermo Fisher Scientific) for 10 min at 4-8 ºC. Each tube was then washed with 100 μL of 1x PBS, centrifuged at 500 g for 5 min at RT, and incubated with 15 μL of a mix of fluorochrome-conjugated anti-mouse monoclonal antibodies (see composition in **Appendix – Supplementary table 5**) for 20 min at RT, followed by a second 1x PBS wash and centrifugation (at 500 g for 5 min at RT). Cell samples were then fixed with 200 μL of 2% formaldehyde for 15 min, retrieved from BSL-3 facility, and further centrifuged (500 g for 5 min at RT) and resuspended in 300 μL of FACS buffer. All samples were subsequently acquired on a e BD LSRFortessa™ X-20 Flow Cytometer and analysed using FlowJo version 10.8.1.

2.6. Statistical analysis

Results are expressed in terms of mean ± standard deviation (SD). Statistical significance of differences between groups were assessed on GraphPad Prism v8 either by employing the Kruskal-Wallis test followed by Dunn's multiple comparisons test or the Mann-Whitney test, depending on the dataset analysed.

3. RESULTS

In order to understand how a primary infection by SARS-CoV-2 impacts the establishment and development of a successful infection by *Plasmodium* parasites, two co-infection models were developed. In our first model, ACE2-humanized mice – the main model used in pre-clinical SARS-CoV-2 infection studies – were primarily exposed to an ancestral variant of SARS-CoV-2 (AnSCV2) and, at different time points, to liver- or blood-infective luciferase-expressing *P. berghei* parasites. The resulting phenotype was thoroughly evaluated before establishing a more attenuated, and thus more versatile and clinically relevant model of SARS-CoV-2 infection. Similarly, this second model consisted in primarily exposing wild-type mice to a mouse-adapted SARS-CoV-2 variant (MA10) and subsequently to liver-infective luciferase-expressing *P. berghei* parasites, with or without allowed progression to the blood stage of infection.

As a first approach, pilot experiments were conducted to assess overall phenotypic changes in both stages of *Plasmodium* infection (see sections 3.1.1 and 3.1.2) and different experimental conditions were explored to obtain the most informative AnSCV2 model. This work thus led to the establishment of an optimized infection scheme, which was employed in all subsequent experimental setups, including in the MA10 model.

3.1 Severe SARS-CoV-2 (AnSCV2) infection model

3.1.1 Co-infection with AnSCV2 and *P. berghei* sporozoites

To determine the specific impact of SARS-CoV-2 on the asymptomatic but obligatory hepatic stage of *P. berghei* infection, ACE2-humanized mice were primarily exposed to AnSCV2, followed by injection of $3x10^4$ *P. berghei* sporozoites, a parasite dose that facilitates the quantification of hepatic infection and its possible variations[111] (**Figure 3.1. A, B**). Two additional groups of mice were single infected with either AnSCV2 or *P. berghei* sporozoites at the same time points as those employed for the co-infected group and used as controls in these experiments. Parasite infection was initially carried out on day 2 post viral inoculation, a time point when viral replication in the lungs is at its peak[95], followed by euthanasia and organ collection 46 h later (**Figure 3.1. A**). Two viral doses, $2.5x10^4$ PFU/50 µL (AnSCV2^{high}) and $1x10^4$ PFU/20 µL (AnSCV2^{low}), were independently tested to assess both whether a decrease in the viral inoculum would delay clinical deterioration in infected mice and its overall effect on *P. berghei*'s liver infection. The final working model was then validated in independent 5-day experiments in which mice were exposed to 3 days of AnSCV2^{low} before being infected with the same dose of *P. berghei* sporozoites (**Figure 3.1. B**).

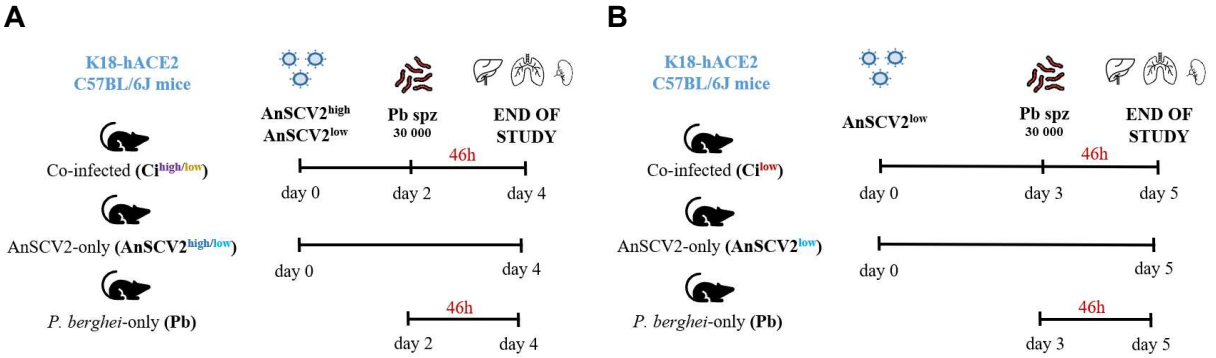

Figure 3.1 – Schematic representation of liver-stage co-infection models. Vertical lines indicate the times points for, respectively, infection with a viral dose of $2.5x10^4$ PFU/50 µL (AnSCV2^{high}) or $1x10^4$ PFU/20 µL (AnSCV2^{low}), infection with $3x10^4$ *P. berghei* sporozoites (Pb spz) two **(A)** or three **(B)** days later, and sacrifice for organ collection 46 h post sporozoite infection.

Co-infected and AnSCV2-single infected mice have similar clinical progression

To evaluate disease progression in mice, body weight and signs of disease were monitored daily (**Figure 3.2. A, B**). As expected for the *Plasmodium* infection stage under evaluation, no clinical signs of disease in *P. berghei*-single infected mice were observed. Conversely, in the two experimental groups exposed to AnSCV2 infection for a total of 4 days (**Figure 3.2. A**), weight loss became apparent on day 3 post viral infection when a higher viral dose was employed, but only at day 4 when a lower viral dose was used, the latter also exhibiting higher body weight percentages than the former at the experimental endpoint. This observation was further validated in a 5-day experimental design (**Figure 3.2. B**) in which all mice exposed to AnSCV2^{low} exhibited stable weight measurements until day 4 and weight losses similar those observed for the higher viral dose (**Figure 3.2. A**) were reached one day later, at day 5 post viral infection. Notably, no significant differences were observed between co-infected and AnSCV2-single infected mice under any experimental condition employed. Collectively, these results indicate that the lower AnSCV2 dose delayed clinical deterioration compared to the higher viral dose, and, most importantly, that subsequent infection with *P. berghei* parasites had no visible impact on the progression of AnSCV2-related disease in either viral dose or time frame employed.

P. berghei hepatic infection has no impact on a previously established AnSCV2 lung infection

To quantify the load of infectious viral particles in the lungs, virus titers were assessed by plaque-forming assay in Vero CCL-81 cells (**Figure 3.2. C**). Overall, no significant differences in lung viral titers were observed between co-infected and AnSCV2-single infected mice in any of the experimental conditions employed. This suggests that the subsequent liver infection by *P. berghei* parasites had no obvious effect on the replication AnSCV2 in the lungs, in accordance to the clinical monitoring results.

A primary AnSCV2 infection attenuates a subsequent *P. berghei* liver infection

Finally, to assess the impact the primary infection with AnSCV2 on the host's susceptibility to a *P. berghei* liver infection, parasite liver load was quantified by RT-qPCR 46 h after sporozoite inoculation (**Figure 3.2. D**). In all experimental conditions, a ~50% reduction in the *P. berghei* liver load was observed in animals previously exposed AnSCV2 infection when compared to *P. berghei*-single infected controls. We thus conclude that liver infection by the malaria parasites was significantly impacted by a primary infection with AnSCV2, independently of viral dose and exposure time employed.

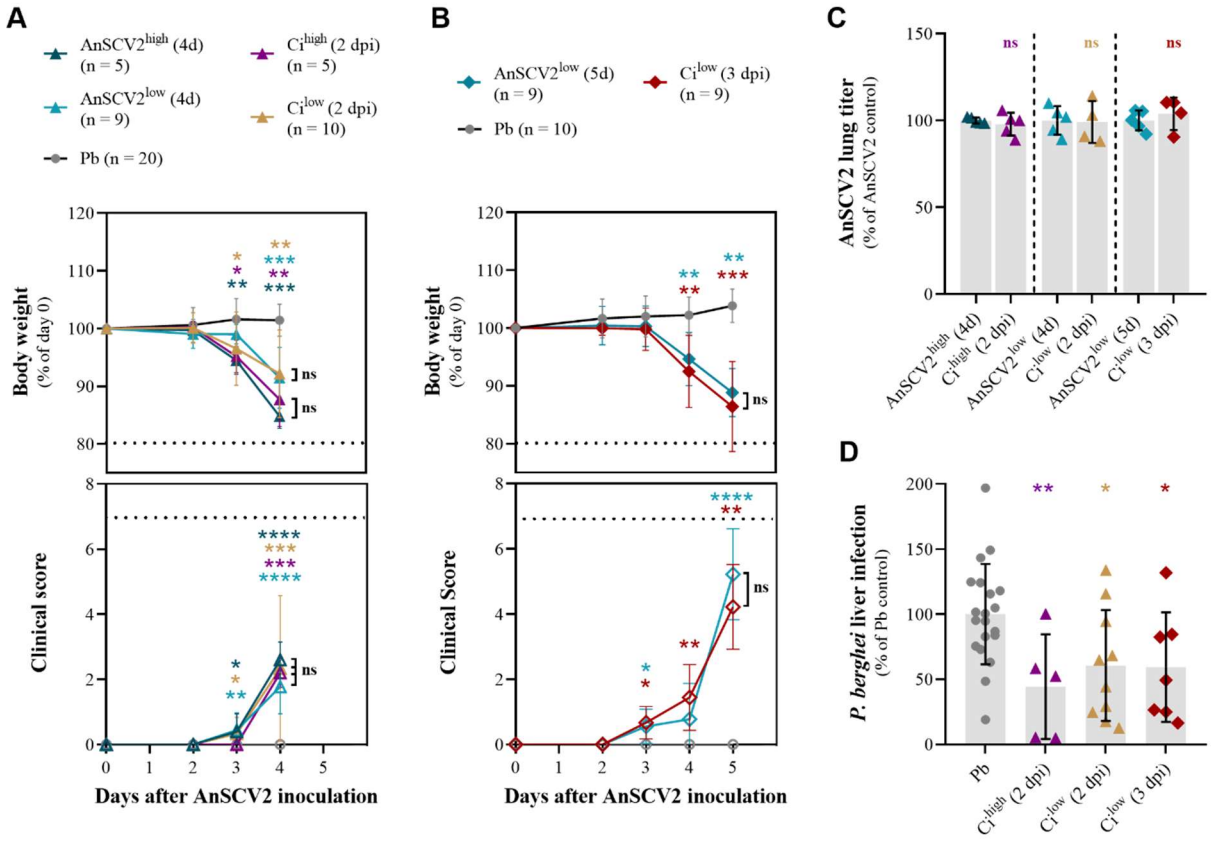

Figure 3.2 – An ongoing AnSCV2 infection attenuates a secondary *P. berghei* liver infection. (A, B) Body weight and clinical signs of disease were monitored daily in all groups. Dotted horizontal lines represent weight percentage threshold for euthanasia (top graph) and maximum value for clinical score (bottom graph). **(C)** AnSCV2 pulmonary infection quantified by virus titration by plaque-forming assay in Vero CCL-81 cells 4 or 5 days post virus inoculation. **(D)** *P. berghei* liver infection quantified by RT-qPCR 46 h after sporozoite injection. Experimental groups include mice exposed to AnSCV2^{high} for 4 days (4d – dark blue) or AnSCV2^{low} for 4 or 5 days (4d – bright blue triangles; 5d – bright blue diamonds), mice infected with *P. berghei* sporozoites 2 or 3 days later (Ci^{high} (2 dpi), Ci^{low} (2 dpi), Ci^{low} (3 dpi) – purple, yellow, and red symbols) and mice only infected with *P. berghei* sporozoites (Pb – grey dots). Single infected mice were used as controls. Each symbol represents mean values for the group (**A** and **B**) or one individual mouse (**C** and **D**) and error bars represent the standard deviation from one to four experiments (n = 5-20 mice per group). The statistical significance of differences between groups from the same experimental condition was assessed by employing the Kruskal-Wallis test followed by Dunn's multiple comparisons test for **A** and **B** and the Mann-Whitney test for **C** and **D** (ns, not significant, * P<0.05, ** P<0.01, *** P<0.001, **** P<0.0001). Coloured asterisks indicate differences relative to the overall phenotypic control group (Pb) and black symbols indicate differences between the remaining experimental groups.

Having observed a decrease in the liver parasite load of co-infected animals relative to their single infected counterparts, we then sought to further characterize the impairment in *P. berghei* liver infection observed in the former. Overall, decreases in the *Plasmodium* liver load are expected to result either from a decrease in the number of parasites that successfully infect hepatocytes and/or from an impairment of the parasite's ability to replicate inside the infected hepatocyte. To assess the contribution of either hypothesis, liver slices collected from co-infected and *P. berghei*-single infected mice were analysed by immunofluorescence microscopy analysis (**Figure 3.3. A**). This analysis revealed that co-infected mice exhibited a significant decrease in the number of *P. berghei*-infected hepatocytes relative to the single infected controls, suggesting that exposure to AnSCV2 either prevented the initial parasitic infection or induced rapid elimination of infected hepatocytes. Notably, no impact on the size of the developing EEFs was observed, indicating that AnSCV2 does not compromise the parasite's intrahepatocytic development. In light of these results, and knowing that AnSCV2 infection induces an exacerbated immune activation in the host, leading to systemic effects – including multiorgan damage[26,27] –, we hypothesised that the inhibitory effect of the virus on *P. berghei* hepatic infection

could be related to unspecific liver damage and/or overall heightened immunosurveillance, both pre- and intra-hepatically. As such, histopathologic analysis of livers collected from all experimental groups was conducted to identify possible alterations in hepatic architecture (**Figure 3.3. B, C**). In accordance with our previous observation (**Figure 3.3. A)**, this analysis revealed that co-infected animals exhibited lower numbers of intrahepatocytic parasite forms than the *P. berghei*-single infected counterparts (**Figure 3.3. B**). However, and most importantly, no marked histopathologic damage nor increased inflammatory cell infiltration was observed in any of the experimental groups, with only co-infected and *P. berghei*-single infected mice exhibiting rare focal inflammatory infiltrates (**Figure 3.3. C**). As such, we conclude that, within the experimental timeframe under evaluation, AnSCV2 exposure did not induce observable hyperinflammation in the liver, indicating that the impairment in liver infection by the malaria parasite could not be attributed to an AnSCV2-mediated exacerbated immune cell infiltration.

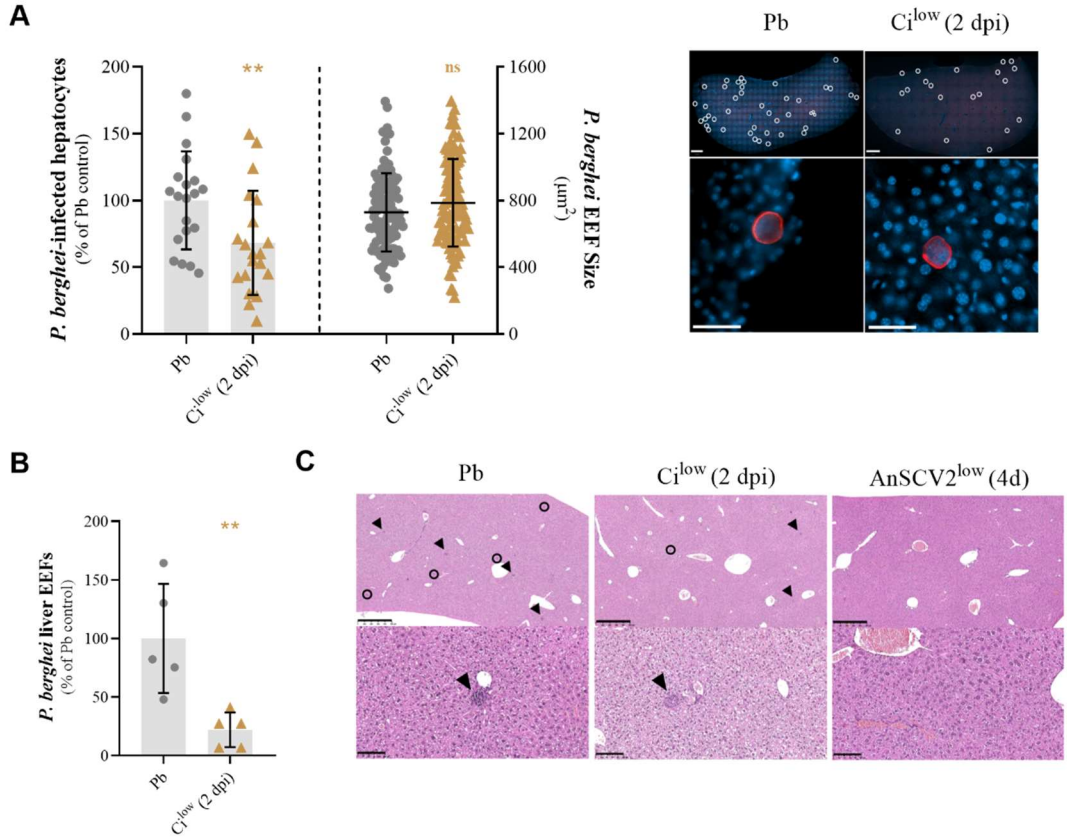

Figure 3.3 - Co-infection decreases the number of *P. berghei*-infected hepatocytes in an inflammation independent way. **(A)** Left: number of *P. berghei*-infected hepatocytes per square centimetre of liver slice (left Y-axis) and size of exoerythrocytic forms (EEF) in square micrometres (right Y-axis), quantified by immunofluorescence microscopy of liver slices from *P. berghei*-single infected mice (Pb – grey dots) and co-infected mice exposed to AnSCV2^{low} two days earlier (Ci^{low} (2 dpi) – yellow dots), 46 h post sporozoite inoculation. Each point represents one liver slice (left Y-axis) or one EEF (right Y-axis), bars (left Y-axis) and horizontal lines (right Y-axis) represent the mean values and error bars the standard deviation of one experiment (n=5 mice per group). Right: representative immunofluorescence microscopy images of whole liver slices (top panels; 1x magnification mosaic; scale bar, 1 mm) and EEFs (bottom panels; 40x magnification; scale bar, 50 µm) from each experimental group. Individual *P. berghei* EEFs are highlighted (white circles; upper panels). Blue: Hoechst (nuclear staining); red: *P. berghei* UIS4 labelling (parasitophorous vacuole membrane). **(B)** Number of *P. berghei* EEFs identified in 10 paraffin embedded liver slides obtained from *P. berghei*-single infected mice (Pb – grey dots) or co-infected mice exposed to AnSCV2^{low} two days earlier (Ci^{low} (2 dpi) – yellow dots). Each point represents one mouse, bars represent the mean values and error bars the standard deviation of one experiment (n=5 mice per group). **(C)** Representative histologic images of *P. berghei*-single, co-infected and AnSCV2-single infected mice. *P. berghei* EEFs (black circles) and inflammatory cell infiltrates (black arrows) are highlighted (upper panels; 5x magnification; scale bar, 500 µm). Microgranulomas (black arrows) composed of mainly mononuclear inflammatory cells are observed in *P. berghei*-only and co-infection conditions, but not in AnSCV2-only infected mice (lower panels; 20x magnification; scale bar, 100 µm). Haematoxylin and eosin. The statistical significance of differences between groups for **A** and **B** was assessed employing the Mann-Whitney test (ns, not significant, ** P<0.01).

On the other hand, to assess the inflammatory events taking place systemically, multi-parameter flow cytometry analysis of mouse spleens was conducted, as a proxy for systemic cell-mediated immune responses (**Appendix – Supplementary figure 1**). Comprehensive analysis of the main cell populations involved in innate and adaptative immunity revealed that the immune landscape of the two AnSCV2-exposed animal groups was generally distinct from that of the *P. berghei*-single infected animals, with co-infected animals developing an immune response that most closely resembles that of their AnSCV2-single infected counterparts (**Figure 3.4. A**, **Appendix – Supplementary figure 2. A**). These results inform us, firstly, that each pathogen induces *per se* a differentiated immune response in the host and, secondly, that parasite infection in mice primarily exposed to AnSCV2 was generally unable to skew the immune responses towards those observed in *P. berghei*-single infected animals. To further scrutinize the responses elicited within the CD4+ helper T and CD8+ cytotoxic T cell compartments, two major populations involved in directed responses against pathogenic infection, naïve (T_N) and antigen experienced T cell phenotypes were analysed (**Figure 3.4. B**). For the latter subset, we focused on the identification of cells expressing central memory (T_{CM}) and effector/effector memory (T_{EM}) phenotypes, as these are the main T cell populations responsible for pathogen control through surveillance of possible infection sites and, in the case of T_{EM} cells, execution of immediate effector functions.[112,113] Our results revealed that both the co-infected and AnSCV2-single infected animals exhibited fewer naïve CD4+ T and CD8+ T cells than *P. berghei*-single infected controls, indicating a clear increase in overall T cell activation in the former. However, this T cell activation in AnSCV2-exposed animals did not directly translate into accumulation of the antigen-experienced counterparts in the spleen, as both CD4+ and CD8+ T_{CM} and T_{EM} subsets were visibly and systematically decreased in co-infected and AnSCV2-single infected animals, relative to the *P. berghei* controls. As such, these results suggest that, in the former two groups, these activated central and effector/effector memory cells were being actively recruited to the periphery at day 5 post AnSCV2 exposure. Notwithstanding, when the proportion of each subset within CD4+ T and CD8+ T cell compartments was analysed (**Appendix – Supplementary figure 2. B**), it became clear that the representation of CD4+ T_{CM} and T_{EM} cell subsets in groups exposed to AnSCV2 infection tended to be increased relative to that of single infected *P. berghei* controls. This result suggests that, although numerically decreased due to cell efflux from the spleen to the periphery, the expansion of these differentiated CD4+ T cells was still being actively stimulated at day 5 post viral infection, indicating that it was a privileged response in the AnSCV2 infected hosts. Moreover, a population of neutrophils was identified in all three groups (**Figure 3.4. A**), with AnSCV2-exposed animals exhibiting a higher proportion of these cells compared to the *P. berghei*-single infected counterparts (**Appendix – Supplementary figure 2. A**). Since these innate cells are not native to the spleen, these results suggest that the 5 days of exposure to AnSCV2 also induced an increase in the population of circulating neutrophils.

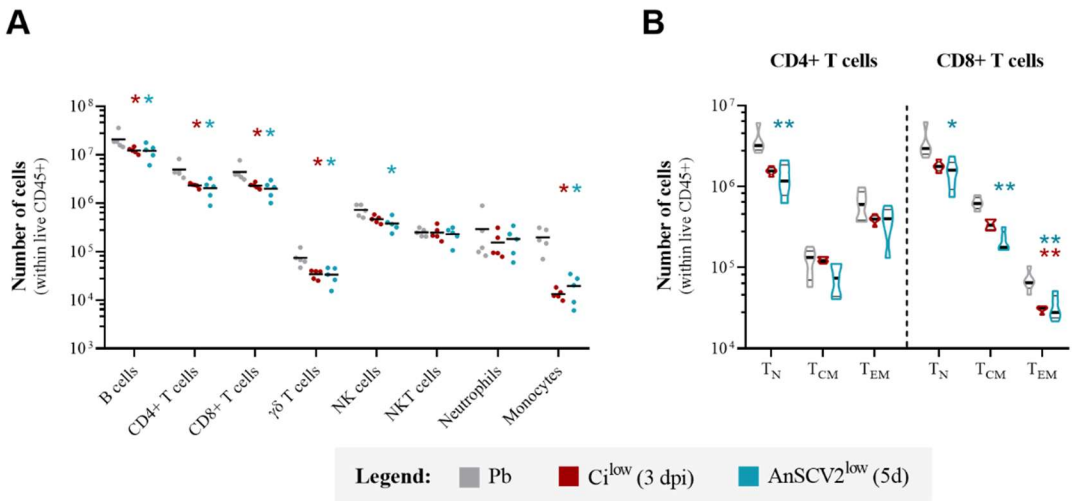

Figure 3.4 – Co-infected animals exhibit an AnSCV2-like immune response. Scatter dot plots for B, CD4+ T, CD8+ T, γδ T, natural killer (NK), natural killer T (NKT), neutrophil and monocyte cell numbers **(A)** and violin plots for the naïve (T_N), central memory (T_{CM}) and effector/effector memory (T_{EM}) population numbers **(B)** within live leukocytes (CD45+), in each condition. Experimental groups include *P. berghei*-single infected mice (Pb – grey symbols), mice exposed to $AnSCV2^{low}$ infection 3 days prior to *P. berghei* inoculation (Ci^{low} (3 dpi) – red symbols) and mice only exposed to a 5-day $AnSCV2^{low}$ infection ($AnSCV2^{low}$ (5d) – bright blue symbols) from one experiment (n = 4-5 mice per group). The statistical significance of differences between groups was assessed by employing the Kruskal-Wallis test followed by Dunn's multiple comparisons test (* P<0.05, ** P<0.01). Coloured asterisks indicate differences relative to the overall phenotypic control group (Pb).

3.1.2 Co-infection with AnSCV2 and *P. berghei*-infected red blood cells

Having observed that a primary infection by AnSCV2 had an inhibitory effect on the asymptomatic liver stage of *P. berghei* infection, we then sought to investigate whether a similar effect would arise during the symptomatic blood stage of infection, independently of pre-hepatic and hepatic events. To this end, the liver stage of the parasite's life cycle was bypassed by directly inoculating $1x10^6$ *P. berghei*-infected red blood cells (iRBCs) into ACE2-humanized mice one day prior to $AnSCV2^{low}$ infection (**Figure 3.4. A**). The time point for iRBC inoculation was defined so that quantifiable parasitaemia levels would be reached at a timepoint after viral infection, thus enabling the assessment of AnSCV2's impact on the early stages of parasite replication in the blood and the subsequent effects on overall blood infection progression. Two independent groups of mice were single-infected with either *P. berghei*-iRBCs or $AnSCV2^{low}$ at the same time points and used as controls. Signs of disease and parasitaemia levels were monitored daily until the experimental endpoint, after which lungs were collected for assessment of viral titers by a plaque-forming assay.

AnSCV2 does not impact *P. berghei*'s replication in the blood

The symptomatic nature of both infections renders the segregation of signs of disease related to either pathogen impossible, particularly considering that both induce general and unspecific signs within the experimental time frame under evaluation. Notwithstanding, our results indicate that each infection induced different degrees of clinical deterioration, with AnSCV2-single infected mice exhibiting faster losses in weight and higher clinical scores when compared with the *P. berghei*-single infected counterparts (**Figure 3.5. B**). Most notably, the co-infected animals appeared to suffer from a faster deterioration than either single-infected control mice, suggesting that co-infection prompts an overall aggravated disease phenotype. However, no differences in end-point lung viral titers (**Figure 3.5. C**) or daily parasitaemias (**Figure 3.5. D**) were found between co-infected and control mice. Collectively, these results indicate not only that *P. berghei*-infection and related pathology did not impact the overall viral replication in the lungs but also that, contrary to what was observed for the liver stage of infection,

exposure to AnSCV2^{low} did not delay or mitigate *P. berghei*'s ability to successfully establish a full-scale blood infection. Furthermore, these results suggest that the concomitant presence of both agents in their clinically active stage of infection leads to an overall aggravated disease phenotype, which appears to be independent of increased viral or parasitic replication.

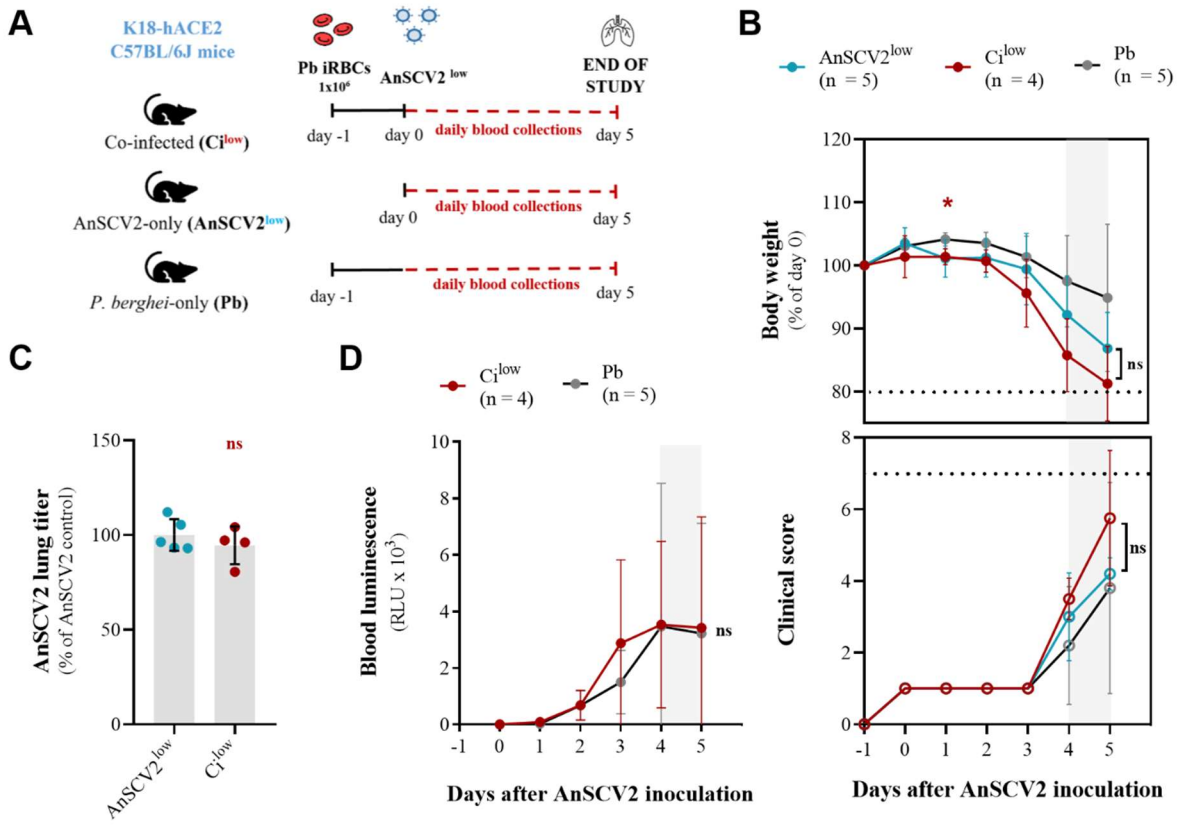

Figure 3.5 – AnSCV2 and blood-stage *P. berghei* infection kinetics are not affected by co-infection. (A) Schematic representation of blood-stage co-infection model. Vertical lines indicate the times points for, respectively, infection with 1x10^6 *P. berghei*-infected red blood cells (Pb iRBCs), infection with a viral dose of 1x10^4 PFU/20 µL (AnSCV2^{low}), and sacrifice for organ collection 5 days later. **(B)** Body weight and clinical signs of disease were monitored daily in all groups. Dotted horizontal lines represent weight percentage threshold for euthanasia (top graph) and maximum value for clinical score (bottom graph). **(C)** AnSCV2 pulmonary infection quantified by virus titration by plaque-forming assay in Vero CCL-81 cells 5 days post virus inoculation. **(D)** *P. berghei* blood infection assessed daily after *P. berghei*-iRBC injection by bioluminescence assay. Grey-shaded areas correspond to the first day of the 5-day ECM development window. Experimental groups include mice exposed to AnSCV2^{low} infection (blue symbols), mice infected with *P. berghei*-iRBCs one day prior (Ci^{low} – red symbols) and mice only infected with *P. berghei*-iRBCs (Pb – grey dots). Single infected mice were used as controls. Each symbol represents mean values for the group (**B** and **D**) or one individual mouse (**C**) and error bars represent the standard deviation from one experiment (n = 4-5 mice per group). The statistical significance of differences between experimental groups was assessed by employing the Kruskal-Wallis test followed by Dunn's multiple comparisons test for **B** and the Mann-Whitney test for **C** and **D** (ns, not significant, * P<0.05). Coloured asterisks indicate differences relative to the overall phenotypic control group (Pb) and black symbols indicate differences between the remaining experimental groups.

3.2. Attenuated SARS-CoV-2 (MA10) model

Our preliminary data showed that primary exposure to AnSCV2 markedly impairs a subsequent hepatic infection by malaria parasites. Despite the relevance of these results, this working model presents some limitations, specifically regarding physiological and clinical relevance, as well as the experimental approaches that it allows. As such, in order to overcome some of these constraints, an alternative infection model based on a mouse-adapted SARS-CoV-2 variant (MA10) was established. Contrary to the AnSCV2 variant, this viral strain is fully capable of infecting wild-type mice, in which it induces a more attenuated non-lethal disease phenotype than the former[114], thus allowing full monitoring of subsequent malaria-associated pathology.

3.2.1 Co-infection with MA10 and a high-dose of *P. berghei* sporozoites

An asymptomatic MA10 infection does not impact a subsequent *P. berghei* liver infection

In order to assess the impact of an ongoing infection by MA10 on a subsequent liver infection by *Plasmodium*, the previously established 5-day liver-stage co-infection model was employed, using wild-type C57BL/6 mice (**Figure 3.6. A**). Interestingly, daily clinical monitoring revealed a total absence of disease signs throughout the experimental timeframe in all three experimental groups, with identical viral replication being observed in both co-infected and MA10-single infected mice, as assessed by plaque-forming assay (**Figure 3.6. B, C**). Importantly, and contrary to previous observations (**Figure 3.2. D**), RT-qPCR analysis of mouse livers indicated no reduction in liver infection by *P. berghei* in co-infected mice compared to *P. berghei*-single infected controls (**Figure 3.6. D**). These results not only confirm the attenuated nature of the MA10 infection model employed, but also indicate that this asymptomatic viral infection did not impact the parasite's liver stage of infection. These results are further validated by the absence of marked systemic immune responses in co-infected and MA10-single infected mice relative to the *P. berghei*-single infected controls (**Appendix – Supplementary figure 3. A, B**).

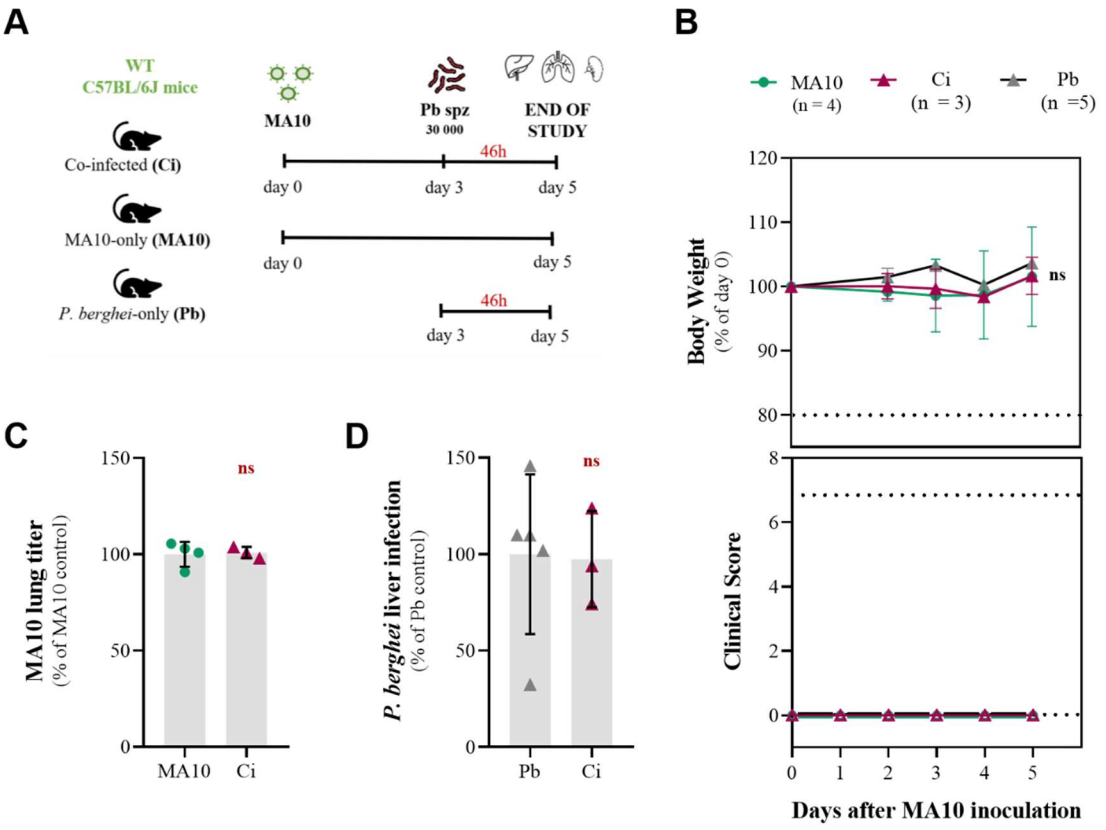

Figure 3.6 – An ongoing asymptomatic MA10 infection does not impact a secondary *P. berghei* liver infection (A) Schematic representation of the attenuated liver-stage co-infection model. Vertical lines indicate time points for, respectively, infection with a viral dose of $1x10^4$ PFU/20 µL (MA10), infection with $3x10^4$ *P. berghei* sporozoites (Pb spz), and sacrifice for organ collection 46 h later. **(B)** Body weight and clinical signs of disease were monitored daily in all groups. Dotted horizontal lines represent weight percentage threshold for euthanasia (top graph) and maximum value for clinical score (bottom graph). **(C)** MA10 pulmonary infection quantified by virus titration by plaque-forming assay in Vero CCL-81 cells 5 days post virus inoculation. **(D)** *P. berghei* liver infection quantified by RT-qPCR 46 h after sporozoite injection. Experimental groups include mice exposed to low-dose MA10 infection (green symbols), mice infected with $3x10^4$ *P. berghei* sporozoites 3 days later (Ci – dark pink symbols) and mice only infected with *P. berghei* sporozoites (Pb – grey symbols). Single infected mice were used as controls. Each symbol represents mean values for the group (**B**) or one individual mouse (**D**) and error bars represent the standard deviation from one experiment (n = 3-5 mice per group). Statistical significance of differences was assessed by employing the Kruskal-Wallis test followed by Dunn's multiple comparisons test in **B** and the Mann-Whitney test in **C** and **D** (ns, not significant).

3.2.2 Co-infection with MA10 and physiological doses of *P. berghei* parasites

In light of these results and knowing that malaria-related outcomes are not determined only by the liver parasite load[115-117], we sought to establish a more physiologically relevant infection model. To this end, wild-type mice were infected with MA10 three days prior to inoculation of 500 liver-infective *P. berghei* parasites, as a surrogate for the inoculum obtained by the bite of five infected mosquitoes[9,111] (**Figure 3.7. A**). In order to evaluate the impact of the asymptomatic viral infection on the subsequent development of malaria-associated pathology, *P. berghei* infection was allowed to proceed into the blood stage, and mouse survival was monitored for at least 10 days after sporozoite infection, a period during which experimental cerebral malaria (ECM) is expected to fully manifest. Clinical monitoring was carried out from day 0 and blood was collected for parasitaemia assessment by bioluminescence from day 5 onward.

An asymptomatic MA10 infection confers partial protection against severe malaria outcomes

Clinical monitoring revealed that all MA10-single infected mice remained asymptomatic and did not succumb to viral infection-related pathology throughout the experimental time frame, only exhibiting short-term arrest in weight gains immediately after viral infection (**Figure 3.7. B**). These results suggest that the mouse-adapted SARS-CoV-2 variant induces transient malaise in infected mice but is overall responsible for an attenuated non-lethal infection, in which the host remains asymptomatic. Conversely, relative to the MA10-single infected controls, both groups of mice exposed to *P. berghei* infection started exhibiting marked weight losses at day 10 of clinical monitoring, a time point inserted within the temporal window during which mice start to succumb to ECM. Moreover, analysis of parasite burden in the blood further revealed that both co-infected and *P. berghei*-single infected mice became concomitantly patent at day 8 of clinical monitoring, exhibiting overall identical parasitaemia levels throughout the experimental time frame (**Figure 3.7. D**). Taken together, and knowing that time to patency serves an indirect indicator of number of merozoites being released from the liver into peripheral circulation[110], these results indicate that exposure to the asymptomatic MA10 infection in the co-infected host did not affect the initial parasite's liver stage of infection nor did it impact its ability to replicate in the blood and establish a full-scale infection. Interestingly, although displaying identical weight loss patterns and parasitaemia levels, the co-infected mice started displaying significant signs of disease one day later than *P. berghei*-single infected animals (**Figure 3.7. B**), the latter also exhibiting an exacerbated disease phenotype throughout the remaining experimental period. Most importantly, our results further demonstrated that the differences observed in clinical phenotypes directly translated into differential survival rates, as *P. berghei*-single infected mice succumbed more to disease within the ECM development window than the co-infected counterparts (**Figure 3.7. C**), with the latter also achieving total symptomatic recovery after day 13 (**Figure 3.7. B**). Collectively, these results suggest that primary exposure to an asymptomatic MA10 infection ultimately conferred some degree of protection against severe malaria pathology and death, and that, interestingly, this protection was independent of parasite burden in the blood.

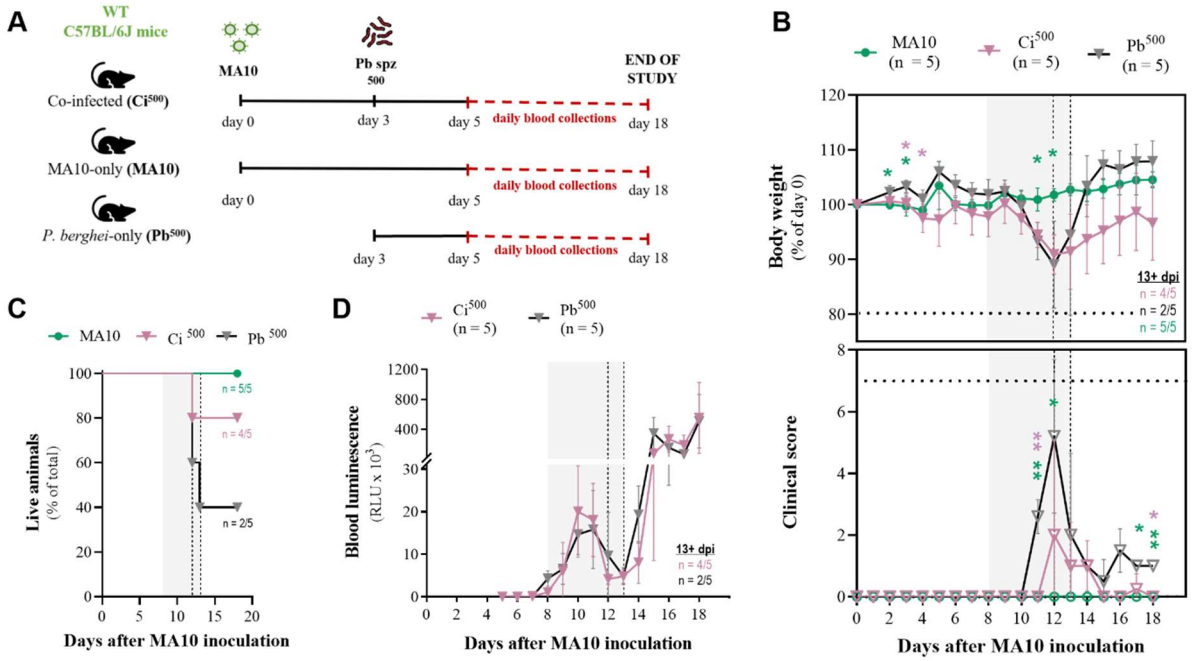

Figure 3.7 – An attenuated SARS-CoV-2 infection partially protects against severe malaria pathology. (A) Schematic representation of the attenuated co-infection model with physiological doses of *Plasmodium* parasites. Vertical lines indicate time points for, respectively, infection with a viral dose of $1x10^4$ PFU/20 µL (MA10), infection with 500 *P. berghei* sporozoites (Pb spz) and start of daily blood collections 46 h post sporozoite infection. **(B, C)** Body weight, clinical signs of disease and mouse survival were monitored daily in all groups. Dotted horizontal lines represent weight threshold for euthanasia (B, top graph) and maximum value for clinical score (B, bottom graph). **(D)** *P. berghei* blood infection quantified by bioluminescence assay from day 5 post MA10 inoculation onwards. Grey-shaded area corresponds to the 5-day ECM development window and vertical dashed lines to time points of mice death (**B**, **C** and **D**). Experimental groups include mice exposed to MA10 infection (green symbols), mice infected with 500 *P. berghei* sporozoites 3 days later (Ci^{500} – light pink symbols) and mice only infected with *P. berghei* sporozoites (Pb^{500} – grey symbols). Single infected mice were used as controls. Each symbol represents mean values for the group and error bars represent the standard deviation from one experiment (n = 5 mice per group). The statistical significance of differences was assessed by employing the Kruskal-Wallis test followed by Dunn's multiple comparisons test in **B**, the Mantel-Cox (log rank) test between Ci^{500} and Pb^{500} in **C** and the Mann-Whitney test in **D** (ns, not significant, * $P<0.05$, ** $P<0.01$). Coloured asterisks indicate differences relative to the Pb group.

4. DISCUSSION

Numerous studies have already demonstrated interactions between *Plasmodium* and other infectious agents, leading to either aggravation[45-48] or attenuation[49-52] of the malaria parasite's pathogenicity. Despite their geographic overlap, the reciprocal impact of concomitant infections by SARS-CoV-2 and *Plasmodium* has not yet been experimentally addressed. Knowing that SARS-CoV-2 infection elicits a marked immune response, we hypothesized that a primary infection by this virus could affect *Plasmodium'*s capacity of successfully establishing an infection and/or influence its natural progression in the host. To test this hypothesis, we developed two co-infection mouse models with distinct SARS-CoV-2 clinical severities. Our results clearly showed that, when a severe disease model of SARS-CoV-2 infection is employed, primary exposure to the virus caused a significant reduction in the subsequent liver infection by the malaria parasite, as measured by RT-qPCR. Immunofluorescence microscopy analysis of livers revealed that the observed impairment was primarily due to a decrease in the number of *Plasmodium*-infected hepatocytes, without an observable impact on their development.

Like in most viral infections, SARS-CoV-2's replication within host cells produces a variety of intermediate viral products that may be recognized as pattern-associated molecular patterns (PAMPs) and subsequently presented to the host's pathogen recognition receptors (PRRs). This interaction activates of a complex array of intracellular signalling cascades that culminate in the production of innate type I and type III interferons (IFNs), the latter being restricted to infections occurring in mucosal barriers, such as the gastrointestinal tract and the lungs.[118] These IFNs are responsible for the upregulation of a plethora of IFN-stimulated genes, leading to the establishment of a cellular state of microbial resistance (cell autonomous immunity) and the production of various cytokines and chemokines involved in the activation of subsequent immune responses.[118-120] These inflammatory mediators are released both locally and systemically, inducing the activation of innate populations in the lungs – such as alveolar macrophages –, while simultaneously recruiting various circulating populations into the infection site, including myeloid and lymphoid subsets, as well as granulocytes.[26,118,121] The recruitment and activation of lymphocytes results in subsequent production of type II IFNs (IFNγ) leading to the establishment of a pro-inflammatory feedback loop in the locally activated populations.[26] Severe disease-causing variants of SARS-CoV-2, like AnSCV2, typically induce a hyper-activation of these inflammatory cascades, an event known as "cytokine storm", leading to generalized responses that systemically affect a plethora of tissues and organs.[26,27,118] Since these inflammatory events are largely recapitulated in the ACE2-humanized murine model employed[95], it can be hypothesised that an AnSCV2-induced immunologic hypervigilance could directly or indirectly mediate rapid clearance of *Plasmodium* parasites following their inoculation, leading to the observed reduction in the proportion of *P. berghei*-infected hepatocytes. This phenomenon can either occur (i) within the liver, where AnSCV2-triggered liver inflammation might mediate rapid identification and elimination of parasites traversing the liver and/or already infecting hepatocytes; or (ii) pre-hepatically, where partial immune-mediated elimination or neutralization of injected malaria parasites could take place. Liver pathology has been reported mainly in COVID-19 patients with severe diseases and includes steatosis and liver inflammation.[122-124] Although generally mild and likely multifactorial in humans, liver abnormalities have been equally reported in some animal models of SARS-CoV-2 infection.[94,125] Despite of the clinically severe disease phenotype induced by infection with AnSCV2, no remarkable signs of inflammatory hepatic lesion were found by histopathologic analysis of liver slices of AnSCV2-infected mice, suggesting that the observed decrease in *Plasmodium* liver infection in co-infected animals was not mediated by an exacerbated immune cell infiltration. Nevertheless, the liver is known to be an immunologically privileged organ since, besides naturally harbouring a diverse set of immune populations – including resident macrophages (Kupfer cells), natural killer (NK), natural killer T (NKT),

CD4+ T, CD8+ T and innate-like T cells –, its distinct anatomical and histologic structure further allows constant and intimate contact between liver cells and the systemically circulating immune mediators.[126,127] These mediators include a vast array of immune populations that regularly patrol liver sinusoids, as well as any soluble inflammatory mediators that might be systemically upregulated.[126] As such, rapid immune responses may be happening near or within the liver milieu without the need for additional cell infiltration into the hepatic parenchyma. For instance, an initially localized inflammatory event involving type I IFNs may ultimately lead to systemic effects in virtually any tissue, as these innate immunity mediators can be produced and perceived, both autocrinally and paracrinally, by most cell types.[120] Knowing that type I IFNs are the main mediators involved in a primary response against liver-stage malaria parasites[128-130] and that their exogenous administration and induction significantly reduces infection during this stage of *Plasmodium* infection[128,131-134], it can be hypothesised that the production of this mediator during AnSCV2 infection might contribute to the observed phenotype. Such an inhibitory effect of type I IFNs on *Plasmodium* liver infection could occur either through the induction of an intrahepatocytic environment unfavourable for the parasite's development (cell autonomous immunity) or by the activation of innate and adaptative immune responses that impair unabridged liver-stage infection. Our results suggest that the former is not implicated in the phenotype observed, as the overall parasite size during intrahepatocytic development was not affected by a primary exposure to AnSCV2 infection. Thus, the most likely mechanism by which AnSCV2 infection decreased parasite liver load is through early and/or enhanced immune cell activation, either systemically or within the liver. Multi-parameter flow cytometry analysis of splenocytes revealed that co-infected animals exhibited an overall AnSCV2-like systemic cellular immune profile, with an obvious increase in neutrophil response and T cell activation, compared to the *P. berghei*-single infected counterparts. Moreover, animals exposed to AnSCV2 exhibited clear signs of peripheral recruitment of both central memory (T_{CM}) and effector/effector memory (T_{EM}) CD4+ T and CD8+ T cells, indicating early activation of the host's adaptative immune cell responses. As mentioned, these cell types are responsible for patrolling possible infection sites in both lymphoid and non-lymphoid tissues, including the blood and all vascular organs, with T_{EM} also executing immediate effector functions within these tissues.[112,113] However, adaptative T cell responses tend to be pathogen-specific, as they normally rely on precise interactions between the T cell receptor (TCR) and its cognate antigen.[135] Nevertheless, memory CD4+ T cells have been described to mediate rapid effector functions in an antigen-unspecific and independent manner, a phenomenon known as "bystander activation", although the same has been deemed unlikely for the CD8+ T cell population in the context of *Plasmodium* infection.[135,136] Knowing that this particular type of activation relies mainly on stimulation of innate cell receptors by unspecific inflammatory mediators, such as cytokines[135,136], it can hypothesised that T cells primarily activated by exposure to AnSCV2 antigens can be subsequently activated by interaction with *Plasmodium*-derived PAMPs, alongside the pro-inflammatory milieu that is concurrently established in the host. However, besides the activation of adaptative immune responses, this AnSCV2-derived hyperinflammatory state could be equally involved in innate immune cell activation. NK and NKT cells, as well as myeloid subsets – like neutrophils and monocytes –, are amongst the innate immune subsets that respond to type I IFN and cytokine stimulation[26,120] and have been implicated in early stages of both viral infection control, including SARS-CoV-2's, as well as in early elimination of liver-stage *Plasmodium* parasite forms.[26,121,136] As such, innate cell populations might also be involved in antigen-independent elimination of liver parasites during co-infection. Noteworthy, the temporal discrepancy between infection with each pathogen means that a more advanced stage of cytokine production is already established when the host is exposed to the malaria parasites. A well-documented example of this is the production IFNγ which has been shown to inhibit *Plasmodium* liver infection.[111,137] Unlike type I IFNs, IFNγ can only be produced at later time points of infection, when lymphocytes become activated.[136,138] Thus, the inflammatory events triggered by primary viral exposure might induce a forward shift in IFNγ

production, which could elicit a plethora of cellular immune responses that would otherwise only be stimulated at later time points of *P. berghei* infection. Overall, the inhibition of *Plasmodium* liver infection by a primary exposure to AnSCV2 might be mediated by a variety of innate and adaptative mechanisms, specifically by either "pre-activating" certain immune cell types that cross-react against incoming parasites in an antigen-unspecific manner, or by creating a pro-inflammatory environment in which the effectiveness of immune responses is globally enhanced.

Although the liver stage of the *Plasmodium* life cycle has been regarded as a critical checkpoint of infection, constituting a bottleneck for its progression into the symptomatic blood stage[136,139], a plethora of significant inflammatory events also take place during the erythrocytic infection cycle, which can be ultimately implicated in the outcomes of disease. Contrary to hepatocytes, red bloods cells (RBCs) are enucleated and are therefore incapable of gene translation and protein production, rendering them ineffective at responding to a vast array of external stimuli, including parasitic infection.[140] As such, neither cell-autonomous immunity nor the classical antigen presentation necessary for initiation of cell-mediated immunity occur during the initial stages of blood infection by *Plasmodium*. However, once the parasite is fully developed and induces the rupture of the host RBC, a variety of *Plasmodium*-derived PAMPs and host cell-derived damage associated molecular patterns (DAMPs) are released into the circulation and may be perceived by the host's innate immune cell types, such as monocytes, neutrophils, dendritic cells (DCs), NK cells and γδ T cells.[116,141-143] This event enables the initiation of type I IFN cascades and the subsequent production of inflammatory mediators, thus establishing a positive feedback loop that further stimulates parasite elimination.[143] Moreover, some of these cells simultaneously function as antigen presenting cells (APCs) capable of activating downstream adaptative immune responses, which culminate not only in further IFN and cytokine release, but also in B-cell mediated antibody production.[142] However, since these events are only initiated after the parasite's full development and replication inside the RBC with subsequent antigen release into circulation, a large-scale blood infection is likely already established before cellular immune responses are generated. Nonetheless, alterations to the parasite's infection dynamics – such as time to patency and blood parasite burden –, or to the host's immune status might influence these temporally restricted inflammatory cascades and ultimately alter the disease outcomes, including the development of severe malaria.[115-117] As such, all these factors should be thoroughly monitored in order to obtain a comprehensive characterization of a *Plasmodium* infection. Our results clearly showed that when the liver stage of *P. berghei* infection is bypassed by direct inoculation of blood stage parasites, co-infected animals exhibited an apparently aggravated disease phenotype, with no differences in viral or parasitic replication. The discrepancy between the observed inhibition of liver-stage infection and the lack of such protective effect during the blood stage could be attributed to multiple factors, including immune responses, parasitaemia levels and model-specific limitations. While type I IFN responses have consistently been proven beneficial during the liver stage of infection, including across different parasite-host combinations, the same is not true for the erythrocytic infection, in which both positive and negative effects of type I IFNs on protection have been reported, depending on the parasite-host combination (as reviewed in [144]). Specifically in the *P. berghei*-C57BL/6 infection model, the effects of type I IFNs on disease outcomes seem to be highly time-dependent. During the first hours after *P. berghei*-iRBC inoculation, type I IFNs remain low, with subsequent increases being associated with suppression of protective immune responses and the development of severe neurologic symptoms.[145-147] Conversely, administration of type I IFNs simultaneously or soon after infection results in a decrease in the levels of some of the major hallmarks of ECM development, such as parasitaemia, pro-inflammatory cytokine levels, sequestration of parasite-infected RBCs and inflammatory mediators in brain microcirculation, as well as decreased expression of adhesion molecules in brain endothelial cells, all of which translate into overall increased host survival.[148-151] Given the temporal specificity of these responses, we can speculate that the time point when co-infected mice were exposed to AnSCV2

infection did not allow the establishment of a significant inflammatory response within the timeframe required to lead to a protective phenotype. Instead, it could even have led to an increase in the levels of these inflammatory mediators within the temporal window during which type I IFNs contribute to malaria-associated pathology[145-147], thus culminating in an additive effect on host neurologic damage. Nevertheless, these results could also be interpreted in light of specific model limitations, as the ACE2-humanized mice employed have been reported to exhibit lethal viral neurodissemination after infection, which is not reported for patients with severe COVID-19 presentations.[152] This viral neurodissemination phenomenon can be attributed to the model's non-physiological overexpression of hACE2 in the mouse brain[152,153] and may question the translational significance of the observed phenotype.

Besides its limited clinical relevance, the ACE2-humanized mouse model, generated on a C57BL/6 genetic background, presents additional constrains as it both (i) hinders the usage of additional knock-out mouse models, that would enable the study of specific host-mediated mechanisms involved in the observed phenotype and (ii) restricts the scope of investigation to experimental cerebral malaria (ECM)-related severe outcomes, precluding the study of the co-infection's impact on other malaria-associated complications, such as hyperparasitaemia or acute respiratory distress syndrome (ARDS). As such, a more relevant model was finally established, using an attenuated mouse-adapted SARS-CoV-2 variant (MA10). Although exposure to MA10 had no effect on the liver stage of *P. berghei* infection, its impact on the outcome of disease was clear. In fact, our results showed that co-infection conferred partial protection from severe neurological symptoms and improved overall survival, compared to *P. berghei*-single infected mice. Interestingly, these effects were independent of any delay in patency or mitigation of the parasite's replication in the blood.

Although some mechanisms of protection against ECM have been preciously studied, most of them relied on either (i) immunization with attenuated *Plasmodium* parasites, with protection against ECM being assessed following challenge with fully virulent parasites;[154-156] or (ii) chemical attenuation of infection during the liver stage of their development[157]. In both cases, an increased time to patency and/or lower parasite burden in the blood was observed. These results are in accordance with the notion that development of ECM is highly dependent on synchronous sequestration of a critical number iRBCs and activated cytotoxic CD8+ T cells within the brain microcirculation, both events depending on specific and time-restricted pro-inflammatory events that are initiated during late-stage intrahepatocytic parasite development.[154,158] As such, the protection against ECM observed in those studies can generally be associated with a decoupling of these two critical events, with cell-mediated inflammatory responses – including CD8+ T cell activation – being stimulated during the liver stage of infection, whilst the subsequent progression and establishment of a blood-stage infection is hampered, thus failing to promptly reach the threshold required for brain inflammatory events to ensue. Although presenting an overall unaltered blood-stage infection, both in terms of time to patency and blood parasite burden, our survival analysis results suggest that a similar mechanism might be involved the observed protection against ECM-related mortality, with primary exposure to viral infection inducing precocious immune activation, thereby equally decoupling these two events. Immune activation and systemic inflammatory responses have been described for MA10 infection, being associated with significant upregulation of a variety inflammatory markers, both in the lungs as well as in the serum of infected mice.[114] These markers included a diversified array of pro-inflammatory cytokines and myeloid- and T cell-associated chemokines involved in the enhancement of inflammatory responses and the recruitment of immune cells to sites of infection, culminating in total resolution of the viral infection. Similarly, one study of COVID-19 patients, reported that, although all patients exhibited upregulation of various inflammatory mediators during the acute phase of infection, asymptomatic or mild disease presentations were specifically associated with higher levels of specific pro-inflammatory cytokines, namely interleukin (IL)-12 and IL-2, when compared to patients with moderate and severe disease.[159] This observation led the authors to conclude that early production of these inflammatory mediators might play a protective

role in COVID-19 pathology. Since these mediators are reportedly increased during infection with the MA10 variant[114], we can hypothesise that the clinically attenuated nature of MA10 infection could be due to the establishment of a more efficacious anti-viral immune response. Moreover, controlled inflammatory responses are also typically dependent on anti-inflammatory cascades and mediators – which are equally upregulated in MA10 models of infection[113] –, being responsible for counteracting hyperactive and deregulated pro-inflammatory events, such as those observed during cytokine storms, thus conferring protection from severe disease outcomes. Likewise, in malaria, besides the type I IFNs addressed above, early production of cytokines such as IL-12 and IL-10, the latter being an important anti-inflammatory mediator, has been associated with protection from ECM in rodent models of infection.[149,160] As such, in co-infected animals, this improved anti-viral immune response might lead to less severe inflammatory events upon *Plasmodium* infection and/or preferentially skew host immune responses towards the control of viral infection in the lungs, possibly leading to partial depletion of innate and adaptative immune populations in circulation. This lower availability of cells could, in turn, translate into a decreased control of parasite replication in the blood – an unlikely possibility given the absence of significant differences in parasitaemia between co-infected and *P. berghei*-single infected animals –, or else lead to lower rates of immune cell sequestration in the brain of co-infected animals. Because circulating CD8+ T cells are indeed involved in anti-viral responses but do not largely contribute to parasite clearance during the blood stage of *Plasmodium* infection, being mainly implicated in the effector phase of ECM development[100,142,143,161], it can be argued that MA10-induced sequestration of these cells to the lungs might protect co-infected animals from severe neurologic damage. Furthermore, an array of other innate cell populations, such as macrophages, DCs and neutrophils, as well as adaptative CD4+ T cells are crucial during the induction phase of ECM, being mainly responsible for cell-cell contacts and production of pro-inflammatory mediators that lead to CD8+ T cell activation.[100,161] As such, any alteration in these populations and their responses may lead to an attenuated ECM phenotype similar to the one observed.

Collectively, our results unveiled a variety of interactions between SARS-CoV-2 and *Plasmodium* infections, with different phenotypes arising depending on the stage of infection and aspect of pathology being analysed. Firstly, we showed that a primary exposure to a variant of the virus that causes severe disease phenotype significantly inhibited a subsequent *P. berghei* hepatic infection, through a reduction in the number of infected hepatocytes and no impairment in overall intrahepatocytic parasite development. We further demonstrated that co-infected animals presented a AnSCV2-like systemic response with enhanced neutrophilic and T cell activation and no direct increase in immune cell infiltration in the liver parenchyma. Such a protection phenotype was not observed when the liver stage of infection was bypassed by direct inoculation of *P. berghei*-iRBCs. However, although exposure to an attenuated variant of SARS-CoV-2 did not reduce a subsequent liver infection by *P. berghei* parasites, it conferred partial protection from severe malaria-associated outcomes and increased overall survival.

To the best of our knowledge, this is the first report to experimentally address the impact of an ongoing SARS-CoV-2 infection on the outcomes of a subsequent *Plasmodium* infection in relevant *in vivo* models. Our results suggest that early inflammatory events triggered by SARS-CoV-2 might induce a rapid identification and elimination of *Plasmodium* liver-stage parasites when an exacerbated anti-microbial response is established. Alternatively, when controlled and effective anti-viral immune responses occur in the lungs, this shift in the localization of immune cell populations might interfere with the establishment of the brain-localized inflammatory events required for the development of ECM. Nonetheless, the specific host factors involved in the observed phenotype remain unknown and should be further addressed. Future experimental approaches should include phenotype assessment in transgenic mice lacking specific candidate genes or immune cell subsets, as well as analysis of tissue-specific inflammatory responses, specifically within the liver, lungs and brain, and the possible

involvement of cytokines and humoral responses. Furthermore, since disease outcomes during the blood stage of the parasite's life cycle are highly dependent on the parasite-host combination employed, different parasite strains and mouse backgrounds should be equally considered. Given the current global epidemiologic status of malaria, co-infections between *Plasmodium* and other pathogens, including respiratory viruses, are bound to occur. As such, our work paves the way for the development of additional co-infection models between *Plasmodium* and viruses responsible for respiratory diseases, thus allowing the elucidation of interactions arising between two major groups of pathogens, in a rigorous and controlled manner, ultimately filling an important knowledge gap regarding complex disease presentations.

REFERENCES

1 White, N. J. in *Manson's Tropical Infectious Diseases (Twenty-third Edition)* (eds Jeremy Farrar *et al.*) Ch. 43, 532-600.e531 (W.B. Saunders, 2014).

2 Coatney, G. R., Collins, W. E., Warren, M. & Contacos, P. G. The primate malarias. (1971).

3 World Health Organization. *World malaria report 2022*. (World Health Organization, 2022).

4 Jeyaprakasam, N. K., Liew, J. W. K., Low, V. L., Wan-Sulaiman, W.-Y. & Vythilingam, I. *Plasmodium knowlesi* infecting humans in Southeast Asia: What's next? *PLOS Neglected Tropical Diseases* **14** https://doi.org:10.1371/journal.pntd.0008900 (2020).

5 Arévalo-Herrera, M. *et al.* Complicated malaria in children and adults from three settings of the Colombian Pacific Coast: A prospective study. *PLOS ONE* **12**, e0185435-e0185435 https://doi.org:10.1371/journal.pone.0185435 (2017).

6 Severe Malaria. *Tropical Medicine & International Health* **19**, 7-131 https://doi.org:https://doi.org/10.1111/tmi.12313_2 (2014).

7 Idro, R., Marsh, K., John, C. C. & Newton, C. R. J. Cerebral malaria: Mechanisms of brain injury and strategies for improved neurocognitive outcome. *Pediatric Research* **68** https://doi.org:10.1203/PDR.0b013e3181eee738 (2010).

8 Bartoloni, A. & Zammarchi, L. Clinical aspects of uncomplicated and severe malaria. *Mediterranean journal of hematology and infectious diseases* **4**, e2012026-e2012026 https://doi.org:10.4084/MJHID.2012.026 (2012).

9 Prudêncio, M., Rodriguez, A. & Mota, M. M. The silent path to thousands of merozoites: the *Plasmodium* liver stage. *Nature Reviews Microbiology* **4**, 849-856 https://doi.org:10.1038/nrmicro1529 (2006).

10 Mota, M. M. *et al.* Migration of *Plasmodium* sporozoites through cells before infection. *Science* **291**, 141-144 https://doi.org:10.1126/science.291.5501.141 (2001).

11 Yang, A. S. P. *et al.* Cell Traversal activity is important for *Plasmodium falciparum* liver infection in humanized mice. *Cell Reports* **18** https://doi.org:10.1016/j.celrep.2017.03.017 (2017).

12 Baer, K., Klotz, C., Kappe, S. H. I., Schnieder, T. & Frevert, U. Release of hepatic *Plasmodium yoelii* merozoites into the pulmonary microvasculature. *PLoS Pathogens* **3**, e171-e171 https://doi.org:10.1371/journal.ppat.0030171 (2007).

13 Venugopal, K., Hentzschel, F., Valkiūnas, G. & Marti, M. *Plasmodium* asexual growth and sexual development in the haematopoietic niche of the host. *Nature Reviews Microbiology* **18**, 177-189 https://doi.org:10.1038/s41579-019-0306-2 (2020).

14 Tandel, N. & Tyagi, R. K. in *Molecular Advancements in Tropical Diseases Drug Discovery* (eds Gauri Misra & Vijay Srivastava) Ch. 5, 95-116 (Academic Press, 2020).

15 Ghebreyesus, T. *WHO Director-General's opening remarks at the media briefing on COVID-19*, https://www.who.int/director-general/speeches/detail/who-director-general-s-opening-remarks-at-the-media-briefing-on-covid-19---11-march-2020 (2022).

16 Gorbalenya, A. E. *et al.* The species Severe acute respiratory syndrome-related coronavirus: classifying 2019-nCoV and naming it SARS-CoV-2. *Nature Microbiology* **5**, 536-544 https://doi.org:10.1038/s41564-020-0695-z (2020).

17 Denison, M. & Becker, M. M. in *Fundamentals of molecular virology* (ed Nicholas H. Acheson) Ch. 14, 159-171 (John Wiley & Sons, 2011).

18 V'kovski, P., Kratzel, A., Steiner, S., Stalder, H. & Thiel, V. Coronavirus biology and replication: implications for SARS-CoV-2. *Nature Reviews Microbiology* **19**, 155-170 https://doi.org:10.1038/s41579-020-00468-6 (2021).

19 Salian, V. S. *et al.* COVID-19 Transmission, current treatment, and future therapeutic strategies. *Molecular Pharmaceutics* **18** https://doi.org:https://doi.org/10.1021/acs.molpharmaceut.0c00608 (2021).

20 Organization, w. H. WHO issues consensus document on the epidemiology of SARS. *Wkly Epidemiol Rec* **78**, 373-375 (2003).

21 de Groot, R. J. *et al.* Middle East respiratory syndrome coronavirus (MERS-CoV): Announcement of the Coronavirus Study Group. *J Virol* **87**, 7790-7792 https://doi.org:10.1128/jvi.01244-13 (2013).

22 Guo, Y.-R. *et al.* The origin, transmission and clinical therapies on coronavirus disease 2019 (COVID-19) outbreak – An update on the status. *Military Medical Research* **7** https://doi.org:10.1186/s40779-020-00240-0 (2020).

23 Holmes, E. C. *et al.* The origins of SARS-CoV-2: A critical review. *Cell* **184** https://doi.org:10.1016/j.cell.2021.08.017 (2021).

24 Wu, Y. *et al.* Incubation Period of COVID-19 caused by unique SARS-CoV-2 strains: A systematic review and meta-analysis. *JAMA Network Open* **5**, e2228008-e2228008 https://doi.org:10.1001/jamanetworkopen.2022.28008 (2022).

25 Merad, M., Blish, C. A., Sallusto, F. & Iwasaki, A. The immunology and immunopathology of COVID-19. *Science* **375**, 1122-1127 https://doi.org:doi:10.1126/science.abm8108 (2022).

26 Boechat, J. L., Chora, I., Morais, A. & Delgado, L. The immune response to SARS-CoV-2 and COVID-19 immunopathology – Current perspectives. *Pulmonology* **27**, 423-437 https://doi.org:https://doi.org/10.1016/j.pulmoe.2021.03.008 (2021).

27 Yang, L. *et al.* The signal pathways and treatment of cytokine storm in COVID-19. *Signal Transduction and Targeted Therapy* **6**, 255-255 https://doi.org:10.1038/s41392-021-00679-0 (2021).

28 *Medical Conditions*, https://www.cdc.gov/coronavirus/2019-ncov/need-extra-precautions/people-with-medical-conditions.html (2022).

29 Greenhalgh, T. *et al.* Ten scientific reasons in support of airborne transmission of SARS-CoV-2. *The Lancet* **397**, 1603-1605 https://doi.org:10.1016/S0140-6736(21)00869-2 (2021).

30 Bestle, D. *et al.* TMPRSS2 and furin are both essential for proteolytic activation of SARS-CoV-2 in human airway cells. *Life Science Alliance* **3**, e202000786-e202000786 https://doi.org:10.26508/lsa.202000786 (2020).

31 Trougakos, I. P. *et al.* Insights to SARS-CoV-2 life cycle, pathophysiology, and rationalized treatments that target COVID-19 clinical complications. *Journal of Biomedical Science* **28**, 9-9 https://doi.org:10.1186/s12929-020-00703-5 (2021).

32 Johnson, B. A. *et al.* Loss of furin cleavage site attenuates SARS-CoV-2 pathogenesis. *Nature* **591**, 293-299 https://doi.org:10.1038/s41586-021-03237-4 (2021).

33 Peacock, T. P. *et al.* The furin cleavage site in the SARS-CoV-2 spike protein is required for transmission in ferrets. *Nature Microbiology* **6**, 899-909 https://doi.org:10.1038/s41564-021-00908-w (2021).

34 Uhlén, M. *et al.* Tissue-based map of the human proteome. *Science* **347**, 1260419 https://doi.org:doi:10.1126/science.1260419 (2015).

35 Gkogkou, E., Barnasas, G., Vougas, K. & Trougakos, I. P. Expression profiling meta-analysis of ACE2 and TMPRSS2, the putative anti-inflammatory receptor and priming protease of SARS-CoV-2 in human cells, and identification of putative modulators. *Redox Biology* **36**, 101615-101615 https://doi.org:10.1016/j.redox.2020.101615 (2020).

36 Poynter, S. J. & DeWitte-Orr, S. J. Understanding viral dsRNA-Mediated innate immune responses at the cellular level using a Rainbow Trout model. *Frontiers in Immunology* **9** https://doi.org:10.3389/fimmu.2018.00829 (2018).

37 Organization, W. H. *The top 10 causes of death*, https://www.who.int/news-room/fact-sheets/detail/the-top-10-causes-of-death (2020).

38 Sachs, J. & Malaney, P. The economic and social burden of malaria. *Nature* **415**, 680-685 https://doi.org:10.1038/415680a (2002).

39 Roll Back Malaria Partnership. The Global Malaria Action Plan for a malaria free world. (World Health Organization, Geneva 2008).

40 World Health Organization. *WHO Coronavirus (COVID-19) Dashboard*, https://covid19.who.int/ (2022).

41 Azarpazhooh, M. R. *et al.* COVID-19 pandemic and burden of non-communicable diseases: an ecological study on data of 185 countries. *Journal of Stroke and Cerebrovascular Diseases* **29**, 105089-105089 https://doi.org:10.1016/j.jstrokecerebrovasdis.2020.105089 (2020).

42 Brief #2: Putting the UN Framework for Socio-Economic Response to COVID-19 into Action: Insights. (2020).

43 McArdle, A. J., Turkova, A. & Cunnington, A. J. When do co-infections matter? *Curr Opin Infect Dis* **31**, 209-215 https://doi.org:10.1097/qco.0000000000000447 (2018).

44 Shen, S.-S., Qu, X.-Y., Zhang, W.-Z., Li, J. & Lv, Z.-Y. Infection against infection: parasite antagonism against parasites, viruses and bacteria. *Infectious Diseases of Poverty* **8**, 49-49 https://doi.org:10.1186/s40249-019-0560-6 (2019).

45 Scott, C. P., Kumar, N., Bishai, W. R. & Manabe, Y. C. Short report: modulation of *Mycobacterium tuberculosis* infection by *Plasmodium* in the murine model. *The American journal of tropical medicine and hygiene* **70** (2004).

46 Normark, J. *et al.* Maladjusted host immune responses induce experimental cerebral malaria-like pathology in a murine *Borrelia* and *Plasmodium* co-infection model. *PLoS ONE* **9** https://doi.org:10.1371/journal.pone.0103295 (2014).

47 Mahittikorn, A., Kotepui, K. U., De Jesus Milanez, G., Masangkay, F. R. & Kotepui, M. A meta-analysis on the prevalence and characteristics of severe malaria in patients with *Plasmodium spp*. and HIV co-infection. *Scientific Reports* **11**, 16655 https://doi.org:10.1038/s41598-021-95591-6 (2021).

48 Mekachie Sandie, S., Sumbele, I. U. N., Tasah, M. M. & Kimbi, H. K. Malaria and intestinal parasite co-infection and its association with anaemia among people living with HIV in Buea, Southwest Cameroon: A community-based retrospective cohort study. *PLoS One* **16**, e0245743 https://doi.org:10.1371/journal.pone.0245743 (2021).

49 Gay, F. *et al.* Helminth infections are associated with protection from cerebral malaria and increased nitrogen derivatives concentrations in Thailand. *The American Journal of Tropical Medicine and Hygiene* **66** https://doi.org:10.4269/ajtmh.2002.66.304 (2002).

50 Page, K. R. *et al. Mycobacterium*-Induced potentiation of type 1 immune responses and protection against malaria are host specific. *Infection and Immunity* **73** https://doi.org:10.1128/IAI.73.12.8369-8380.2005 (2005).

51 Lemaitre, M. *et al.* Coinfection with *Plasmodium falciparum* and *Schistosoma haematobium*: additional evidence of the protective effect of schistosomiasis on malaria in Senegalese children. *Am J Trop Med Hyg* **90**, 329-334 https://doi.org:10.4269/ajtmh.12-0431 (2014).

52 Davenport, G. C. *et al.* Reduced parasite burden in children with falciparum malaria and bacteremia coinfections: Role of mediators of inflammation. *Mediators of Inflammation* **2016** https://doi.org:10.1155/2016/4286576 (2016).

53 Figueiredo, I. R. d., Martins, M., Midões, C. & Ferrão, J. B. Opportunistic infections in the immunocompromised: HIV *vs* non-HIV patients - A narrative review. *Medical Research Archives* **10** https://doi.org:10.18103/mra.v10i6.2887 (2022).

54 Diou, J., Tardif, M. R., Barat, C. & Tremblay, M. J. Dendritic cells derived from hemozoin-loaded monocytes display a partial maturation phenotype that promotes HIV-1 trans-infection of CD4+ T cells and virus replication. *The Journal of Immunology* **184** https://doi.org:10.4049/jimmunol.0901513 (2010).

55 Orlov, M. *et al.* Antigen-presenting phagocytic cells ingest malaria parasites and increase HIV replication in a tumor necrosis factor α-dependent manner. *The Journal of infectious diseases* **210**, 1562-1572 https://doi.org:10.1093/infdis/jiu317 (2014).

56 Hochman, S. & Kim, K. The Impact of HIV Coinfection on cerebral malaria pathogenesis. *Journal of neuroparasitology* **3**, 235547-235547 https://doi.org:10.4303/jnp/235547 (2012).

57 Berg, A. *et al.* Increased severity and mortality in adults co-infected with malaria and HIV in Maputo, Mozambique: A prospective cross-sectional study. *PloS one* **9**, e88257-e88257 https://doi.org:10.1371/journal.pone.0088257 (2014).

58 World Health Organization. *Global tuberculosis report 2021*. (World Health Organization, 2021).

59 Tékpa, G. *et al.* Aspects épidémiologiques et cliniques de la tuberculose en milieu hospitalier à Bangui. *Pan African Medical Journal* **33** https://doi.org:10.11604/pamj.2019.33.31.13442 (2019).

60 Valadas, E. *et al.* Tuberculosis with malaria or HIV co-infection in a large hospital in Luanda, Angola. *The Journal of Infection in Developing Countries* **7**, 269-272 https://doi.org:10.3855/jidc.2703 (2013).

61 C. Enwere, M. O. O. S. K. O. G. The host response in malaria and depression of defence against tuberculosis. *Annals of Tropical Medicine And Parasitology* **93**, 669-678 https://doi.org:10.1080/00034989957907 (1999).

62 Li, X.-X. & Zhou, X.-N. Co-infection of tuberculosis and parasitic diseases in humans: a systematic review. *Parasites & Vectors* **6**, 79-79 https://doi.org:10.1186/1756-3305-6-79 (2013).

63 Whittaker, E., López-Varela, E., Broderick, C. & Seddon, J. A. Examining the complex relationship between tuberculosis and other infectious diseases in children. *Frontiers in Pediatrics* **7** https://doi.org:10.3389/fped.2019.00233 (2019).

64 Mueller, A. K., Behrends, J., Blank, J., Schaible, U. E. & Schneider, B. E. An experimental model to study tuberculosis-malaria coinfection upon natural transmission of *Mycobacterium tuberculosis* and *Plasmodium berghei*. *J Vis Exp*, e50829 https://doi.org:10.3791/50829 (2014).

65 Smrkovski, L. L. & Strickland, G. T. Rodent malaria: BCG-induced protection and immunosuppression. *J Immunol* **121**, 1257-1261 (1978).

66 Yazdanbakhsh, M. & Kremsner, P. G. Influenza in Africa. *PLoS Med* **6**, e1000182 https://doi.org:10.1371/journal.pmed.1000182 (2009).

67 Gessner, B. D., Shindo, N. & Briand, S. Seasonal influenza epidemiology in sub-Saharan Africa: a systematic review. *Lancet Infect Dis* **11**, 223-235 https://doi.org:10.1016/s1473-3099(11)70008-1 (2011).

68 Niang, M. N. *et al.* Viral etiology of respiratory infections in children under 5 years old living in tropical rural areas of Senegal: The EVIRA project. *Journal of Medical Virology* **82**, 866-872 https://doi.org:10.1002/jmv.21665 (2010).

69 Nzoumbou-Boko, R. *et al.* Falciparum malaria in febrile patients at sentinel sites for influenza surveillance in the Central African Republic from 2015 to 2018. *Interdisciplinary Perspectives on Infectious Diseases* **2020**, 1-7 https://doi.org:10.1155/2020/3938541 (2020).

70 Waitumbi, J. N. *et al.* Outpatient upper respiratory tract viral infections in children with malaria symptoms in Western Kenya. *The American journal of tropical medicine and hygiene* **83**, 1010-1013 https://doi.org:10.4269/ajtmh.2010.10-0174 (2010).

71 Thompson, M. G. *et al.* Influenza and malaria coinfection among young children in western Kenya, 2009-2011. *The Journal of infectious diseases* **206**, 1674-1684 https://doi.org:10.1093/infdis/jis591 (2012).

72 Peterson, I. *et al.* Respiratory virus-associated severe acute respiratory illness and viral clustering in Malawian children in a setting with a high prevalence of HIV infection, malaria, and malnutrition. *The Journal of infectious diseases* **214**, 1700-1711 https://doi.org:10.1093/infdis/jiw426 (2016).

73 Kishore, R. *et al.* COVID-19: Possible cause of induction of relapse of *Plasmodium vivax* infection. *The Indian Journal of Pediatrics* **87**, 751-752 https://doi.org:10.1007/s12098-020-03441-6 (2020).

74 Sardar, S., Sharma, R., Alyamani, T. Y. M. & Aboukamar, M. COVID-19 and *Plasmodium vivax* malaria co-infection. *IDCases* **21**, e00879-e00879 https://doi.org:https://doi.org/10.1016/j.idcr.2020.e00879 (2020).

75 Caglar, B., Karaali, R., Balkan, I. I., Mete, B. & Aygun, G. COVID-19 and *Plasmodium ovale* malaria: A rare case of co-infection. *The Korean Journal of Parasitology* **59**, 399-402 https://doi.org:10.3347/kjp.2021.59.4.399 (2021).

76 Eid, M. M. Co-Infection with COVID-19 and malaria in a young man. *Dubai Medical Journal* **4**, 164-166 https://doi.org:10.1159/000514254 (2021).

77 Indari, O. *et al.* Insights into *Plasmodium* and SARS-CoV-2 co-infection driven neurological manifestations. *Biosafety and Health* **3**, 230-234 https://doi.org:10.1016/j.bsheal.2021.04.001 (2021).

78 Jochum, J. *et al.* Malaria in the time of COVID-19: Do not miss the real cause of illness. *Tropical Medicine and Infectious Disease* **6**, 40-40 https://doi.org:10.3390/tropicalmed6020040 (2021).

79 Pusparani, A., Henrina, J. & Cahyadi, A. Co-infection of COVID-19 and recurrent malaria. *The Journal of Infection in Developing Countries* **15**, 625-629 https://doi.org:10.3855/jidc.13793 (2021).

80 Shahid, Z., Karim, N., Shahid, F. & Yousaf, Z. COVID-19 associated imported *Plasmodium vivax* malaria relapse: First reported case and literature review. *Research and Reports in Tropical Medicine* **Volume 12**, 77-80 https://doi.org:10.2147/RRTM.S292157 (2021).

81 Hussein, R. *et al.* Impact of COVID-19 and malaria coinfection on clinical outcomes: a retrospective cohort study. *Clinical Microbiology and Infection* **28**, 1152.e1151-1152.e1156 https://doi.org:https://doi.org/10.1016/j.cmi.2022.03.028 (2022).

82 Wilairatana, P., Masangkay, F. R., Kotepui, K. U., Milanez, G. D. J. & Kotepui, M. Prevalence and characteristics of malaria among COVID-19 individuals: A systematic review, meta-analysis, and analysis of case reports. *PLOS Neglected Tropical Diseases* **15**, e0009766-e0009766 https://doi.org:10.1371/journal.pntd.0009766 (2021).

83 Anyanwu, M. U. The association between malaria prevalence and COVID-19 mortality. *BMC Infectious Diseases* **21** https://doi.org:10.1186/s12879-021-06701-8 (2021).

84 Raham, T. F. Influence of malaria endemicity and tuberculosis prevalence on COVID-19 mortality. *Public Health* **194**, 33-35 https://doi.org:10.1016/j.puhe.2021.02.018 (2021).

85 Achan, J. *et al.* Current malaria infection, previous malaria exposure, and clinical profiles and outcomes of COVID-19 in a setting of high malaria transmission: an exploratory cohort study in Uganda. *The Lancet Microbe* **3**, e62-e71 https://doi.org:10.1016/S2666-5247(21)00240-8 (2022).

86 World Health Organization. *The Malaria Atlas Project*, https://data.malariaatlas.org/maps?layers=Malaria:202206_Global_Pv_Incidence_Rate,Malaria:202206_Global_Pf_Incidence_Rate (2022).

87 Prudêncio, M., Mota, M. M. & Mendes, A. M. A toolbox to study liver stage malaria. *Trends in Parasitology* **27**, 565-574 https://doi.org:10.1016/j.pt.2011.09.004 (2011).

88 de Oca, M. M., Engwerda, C. & Haque, A. in *Mouse Models of Innate Immunity* (ed Irving C. Allen) Ch. 23, 203-213 (2013).

89 Thyagarajan, T., Totey, S., Danton, M. J. S. & Kulkarni, A. B. Genetically altered mouse models: the good, the bad, and the ugly. *Critical Reviews in Oral Biology & Medicine* **14**, 154-174 https://doi.org:10.1177/154411130301400302 (2003).

90 Gurumurthy, C. B. & Lloyd, K. C. K. Generating mouse models for biomedical research: technological advances. *Disease Models & Mechanisms* **12** https://doi.org:10.1242/dmm.029462 (2019).

91 Walsh, N. C. *et al.* Humanized mouse models of clinical disease. *Annual Review of Pathology: Mechanisms of Disease* **12**, 187-215 https://doi.org:10.1146/annurev-pathol-052016-100332 (2017).

92 Minkah, N. K., Schafer, C. & Kappe, S. H. I. Humanized mouse models for the study of human malaria parasite biology, Pathogenesis, and Immunity. *Frontiers in Immunology* **9** https://doi.org:10.3389/fimmu.2018.00807 (2018).

93 Bao, L. *et al.* The pathogenicity of SARS-CoV-2 in hACE2 transgenic mice. *Nature* **583**, 830-833 https://doi.org:10.1038/s41586-020-2312-y (2020).

94 Yinda, C. K. *et al.* K18-hACE2 mice develop respiratory disease resembling severe COVID-19. *bioRxiv : the preprint server for biology* https://doi.org:10.1101/2020.08.11.246314 (2020).

95 Winkler, E. S. *et al.* SARS-CoV-2 infection of human ACE2-transgenic mice causes severe lung inflammation and impaired function. *Nature Immunology* **21**, 1327-1335 https://doi.org:10.1038/s41590-020-0778-2 (2020).

96 Diamond, M. *et al.* The SARS-CoV-2 B.1.1.529 omicron virus causes attenuated infection and disease in mice and hamsters. *Research square* https://doi.org:10.21203/rs.3.rs-1211792/v1 (2021).

97 Mota, M. M. & Rodriguez, A. *Malaria: Immune response to infection and vaccination*. (Springer International Publishing, 2017).

98 Wykes, M. N. & Good, M. F. What have we learnt from mouse models for the study of malaria? *European Journal of Immunology* **39**, 2004-2007 https://doi.org:10.1002/eji.200939552 (2009).

99 Huang, B. W., Pearman, E. & Kim, C. C. Mouse models of uncomplicated and fatal malaria. *Bio-protocol* **5** https://doi.org:10.21769/bioprotoc.1514 (2015).

100 Ghazanfari, N., Mueller, S. N. & Heath, W. R. Cerebral malaria in mouse and man. *Frontiers in Immunology* **9** https://doi.org:10.3389/fimmu.2018.02016 (2018).

101 Dehghan, H. *et al.* Experimental study on *Plasmodium berghei*, *Anopheles Stephensi*, and BALB/c mouse system: Implications for malaria transmission blocking assays. *Iran J Parasitol* **13**, 549-559 (2018).

102 Scheller, L. F., Wirtz, R. A. & Azad, A. F. Susceptibility of different strains of mice to hepatic infection with *Plasmodium berghei*. *Infection and immunity* **62**, 4844-4847 https://doi.org:10.1128/iai.62.11.4844-4847.1994 (1994).

103 Franke-Fayard, B. et al. Murine malaria parasite sequestration: CD36 is the major receptor, but cerebral pathology is unlinked to sequestration. *Proc Natl Acad Sci U S A* **102**, 11468-11473 https://doi.org:10.1073/pnas.0503386102 (2005).

104 Ploemen, I. H. J. *et al.* Visualisation and quantitative analysis of the rodent malaria liver stage by real time imaging. *PLoS ONE* **4** https://doi.org:10.1371/journal.pone.0007881 (2009).

105 Douradinha, B. *et al.* Genetically attenuated P36p-deficient *Plasmodium berghei* sporozoites confer long-lasting and partial cross-species protection. *International Journal for Parasitology* **37**, 1511-1519 https://doi.org:10.1016/j.ijpara.2007.05.005 (2007).

106 Moreau, G. B. *et al.* Evaluation of K18-hACE2 mice as a model of SARS-CoV-2 infection. *Am J Trop Med Hyg* **103**, 1215-1219 https://doi.org:10.4269/ajtmh.20-0762 (2020).

107 Mendes, A. M. *et al.* Inhibition of *Plasmodium* liver infection by Ivermectin. *Antimicrobial Agents and Chemotherapy* **61**, e02005-02016 https://doi.org:doi:10.1128/AAC.02005-16 (2017).

108 Bruña-Romero, O. *et al.* Detection of malaria liver-stages in mice infected through the bite of a single *Anopheles* mosquito using a highly sensitive real-time PCR. *International Journal for Parasitology* **31** https://doi.org:10.1016/S0020-7519(01)00265-X (2001).

109 Green, M. & Sambrook, J. in *Molecular Cloning: A Laboratory Manual* Vol. 1 (eds Judy Cuddihy, Kaaren Janssen, Michael Zierler, & Kathleen Bubbeo) Ch. 6.7, 372-374 (John Inglis, 2012).

110 Zuzarte-Luis, V., Sales-Dias, J. & Mota, M. M. Simple, sensitive and quantitative bioluminescence assay for determination of malaria pre-patent period. *Malaria Journal* **13**, 15 https://doi.org:10.1186/1475-2875-13-15 (2014).

111 Sanches-Vaz, M. *et al. Trypanosoma brucei* infection protects mice against malaria. *PLOS Pathogens* **15**, e1008145 https://doi.org:10.1371/journal.ppat.1008145 (2019).

112 Sallusto, F., Geginat, J. & Lanzavecchia, A. Central memory and effector memory T cell subsets: Function, generation, and maintenance. *Annual Review of Immunology* **22**, 745-763 https://doi.org:10.1146/annurev.immunol.22.012703.104702 (2004).

113 Jameson, S. C. & Masopust, D. Understanding subset diversity in T cell memory. *Immunity* **48**, 214-226 https://doi.org:10.1016/j.immuni.2018.02.010 (2018).

114 Leist, S. R. *et al.* A Mouse-adapted SARS-CoV-2 induces acute lung injury and mortality in standard laboratory mice. *Cell* **183**, 1070-1085.e1012 https://doi.org:10.1016/j.cell.2020.09.050 (2020).

115 Hunt, N. H. & Grau, G. E. Cytokines: accelerators and brakes in the pathogenesis of cerebral malaria. *Trends Immunol* **24**, 491-499 https://doi.org:10.1016/s1471-4906(03)00229-1 (2003).

116 Stevenson, M. M. & Riley, E. M. Innate immunity to malaria. *Nature Reviews Immunology* **4**, 169-180 https://doi.org:10.1038/nri1311 (2004).

117 McQuillan, J. A. *et al.* Coincident parasite and CD8 T cell sequestration is required for development of experimental cerebral malaria. *Int J Parasitol* **41**, 155-163 https://doi.org:10.1016/j.ijpara.2010.08.003 (2011).

118 Ramasamy, S. & Subbian, S. Critical determinants of cytokine storm and type I interferon response in COVID-19 pathogenesis. *Clinical Microbiology Reviews* **34**, e00299-00220 https://doi.org:doi:10.1128/CMR.00299-20 (2021).

119 MacMicking, J. D. Interferon-inducible effector mechanisms in cell-autonomous immunity. *Nature Reviews Immunology* **12**, 367-382 https://doi.org:10.1038/nri3210 (2012).

120 Ivashkiv, L. B. & Donlin, L. T. Regulation of type I interferon responses. *Nature Reviews Immunology* **14**, 36-49 https://doi.org:10.1038/nri3581 (2014).

121 Primorac, D. *et al.* Adaptive immune responses and immunity to SARS-CoV-2. *Frontiers in Immunology* **13** https://doi.org:10.3389/fimmu.2022.848582 (2022).

122 Wang, Y. *et al.* SARS-CoV-2 infection of the liver directly contributes to hepatic impairment in patients with COVID-19. *Journal of Hepatology* **73**, 807-816 https://doi.org:10.1016/j.jhep.2020.05.002 (2020).

123 Chornenkyy, Y. *et al.* Liver pathology and SARS-CoV-2 detection in formalin-fixed tissue of patients with COVID-19. *American Journal of Clinical Pathology* **155**, 802-814 https://doi.org:10.1093/ajcp/aqab009 (2021).

124 Marjot, T. *et al.* COVID-19 and liver disease: mechanistic and clinical perspectives. *Nature Reviews Gastroenterology & Hepatology* **18**, 348-364 https://doi.org:10.1038/s41575-021-00426-4 (2021).

125 Shou, S. *et al.* Animal models for COVID-19: Hamsters, mouse, ferret, mink, tree shrew, and non-human primates. *Frontiers in Microbiology* **12** https://doi.org:10.3389/fmicb.2021.626553 (2021).

126 Robinson, M. W., Harmon, C. & O'Farrelly, C. Liver immunology and its role in inflammation and homeostasis. *Cellular & Molecular Immunology* **13**, 267-276 https://doi.org:10.1038/cmi.2016.3 (2016).

127 Freitas-Lopes, M. A., Mafra, K., David, B. A., Carvalho-Gontijo, R. & Menezes, G. B. Differential location and distribution of hepatic immune cells. *Cells* **6** https://doi.org:10.3390/cells6040048 (2017).

128 Liehl, P. *et al.* Host-cell sensors for *Plasmodium* activate innate immunity against liver-stage infection. *Nature Medicine* **20**, 47-53 https://doi.org:10.1038/nm.3424 (2014).

129 Miller, Jessica L., Sack, Brandon K., Baldwin, M., Vaughan, Ashley M. & Kappe, Stefan H. I. Interferon-mediated innate immune responses against malaria parasite liver stages. *Cell Reports* **7**, 436-447 https://doi.org:10.1016/j.celrep.2014.03.018 (2014).

130 Liehl, P. *et al.* Innate immunity induced by *Plasmodium* liver infection inhibits malaria reinfections. *Infect Immun* **83**, 1172-1180 https://doi.org:10.1128/iai.02796-14 (2015).

131 Jahiel, R. I., Vilček, J., Nussenzweig, R. & Vanderberg, J. Interferon inducers protect mice against *Plasmodium berghei* malaria. *Science* **161**, 802-804 https://doi.org:doi:10.1126/science.161.3843.802 (1968).

132 Jahiel, R. I., Nussenzweig, R. S., Vanderberg, J. & VilČEk, J. A. N. Anti-malarial effect of interferon inducers at different stages of development of *Plasmodium berghei* in the mouse. *Nature* **220**, 710-711 https://doi.org:10.1038/220710a0 (1968a).

133 Jahiel, R. I., Vilcek, J. A. N. & Nussenzweig, R. S. Exogenous interferon protects mice against *Plasmodium berghei* malaria. *Nature* **227**, 1350-1351 https://doi.org:10.1038/2271350a0 (1970).

134 Emran, T. B. *et al. Baculovirus*-induced fast-acting innate immunity kills liver-stage *Plasmodium*. *J Immunol* **201**, 2441-2451 https://doi.org:10.4049/jimmunol.1800908 (2018).

135 Lee, H.-G., Cho, M.-Z. & Choi, J.-M. Bystander CD4+ T cells: Crossroads between innate and adaptive immunity. *Experimental & Molecular Medicine* **52**, 1255-1263 https://doi.org:10.1038/s12276-020-00486-7 (2020).

136 Holz, L. E., Fernandez-Ruiz, D. & Heath, W. R. Protective immunity to liver-stage malaria. *Clin Transl Immunology* **5**, e105 https://doi.org:10.1038/cti.2016.60 (2016).

137 Schofield, L. *et al.* Gamma interferon, CD8+ T cells and antibodies required for immunity to malaria sporozoites. *Nature* **330**, 664-666 https://doi.org:10.1038/330664a0 (1987).

138 Schoenborn, J. R. & Wilson, C. B. Regulation of interferon-gamma during innate and adaptive immune responses. *Adv Immunol* **96**, 41-101 https://doi.org:10.1016/s0065-2776(07)96002-2 (2007).

139 Graumans, W., Jacobs, E., Bousema, T. & Sinnis, P. When is a *Plasmodium*-infected mosquito an infectious mosquito? *Trends in Parasitology* **36**, 705-716 https://doi.org:10.1016/j.pt.2020.05.011 (2020).

140 Anderson, H. L., Brodsky, I. E. & Mangalmurti, N. S. The Evolving Erythrocyte: Red Blood Cells as Modulators of Innate Immunity. *The Journal of Immunology* **201**, 1343-1351 https://doi.org:10.4049/jimmunol.1800565 (2018).

141 Götz, A. *et al.* in *Malaria: Immune Response to Infection and Vaccination* (eds Maria M. Mota & Ana Rodriguez) 3-25 (Springer International Publishing, 2017).

142 Wykes, M. N., Stephens, R. & Cockburn, I. A. in *Malaria: Immune Response to Infection and Vaccination* (eds Maria M. Mota & Ana Rodriguez) 47-66 (Springer International Publishing, 2017).

143 Bucşan, A. N. & Williamson, K. C. Setting the stage: The initial immune response to blood-stage parasites. *Virulence* **11**, 88-103 https://doi.org:10.1080/21505594.2019.1708053 (2020).

144 He, X., Xia, L., Tumas, K. C., Wu, J. & Su, X. Z. Type I interferons and malaria: A double-edge sword against a complex parasitic disease. *Front Cell Infect Microbiol* **10**, 594621 https://doi.org:10.3389/fcimb.2020.594621 (2020).

145 Haque, A. *et al.* Type I interferons suppress CD4+ T-cell-dependent parasite control during blood-stage *Plasmodium* infection. *European Journal of Immunology* **41**, 2688-2698 https://doi.org:https://doi.org/10.1002/eji.201141539 (2011).

146 Haque, A. *et al.* Type I IFN signaling in CD8– DCs impairs Th1-dependent malaria immunity. *The Journal of Clinical Investigation* **124**, 2483-2496 https://doi.org:10.1172/JCI70698 (2014).

147 Tamura, T., Kimura, K., Yui, K. & Yoshida, S. Reduction of conventional dendritic cells during *Plasmodium* infection is dependent on activation induced cell death by type I and II interferons. *Exp Parasitol* **159**, 127-135 https://doi.org:10.1016/j.exppara.2015.09.010 (2015).

148 Vigário, A. M. *et al.* Inhibition of *Plasmodium yoelii* blood-stage malaria by interferon alpha through the inhibition of the production of its target cell, the reticulocyte. *Blood* **97**, 3966-3971 https://doi.org:10.1182/blood.v97.12.3966 (2001).

149 Mitchell, A. J. *et al.* Early cytokine production is associated with protection from murine cerebral malaria. *Infect Immun* **73**, 5645-5653 https://doi.org:10.1128/iai.73.9.5645-5653.2005 (2005).

150 Vigário, A. M. *et al.* Recombinant human IFN-α inhibits cerebral malaria and reduces parasite burden in mice. *The Journal of Immunology* **178**, 6416-6425 https://doi.org:10.4049/jimmunol.178.10.6416 (2007).

151 Morrell, C. N. *et al.* Beta Interferon suppresses the development of experimental cerebral malaria. *Infection and Immunity* **79**, 1750-1758 https://doi.org:doi:10.1128/IAI.00810-10 (2011).

152 Carossino, M. *et al.* Fatal neurodissemination and SARS-CoV-2 tropism in K18-hACE2 mice is only partially dependent on hACE2 expression. *Viruses* **14** https://doi.org:10.3390/v14030535 (2022).

153 McCray, P. B. *et al.* Lethal Infection of K18-hACE2 mice infected with severe acute respiratory syndrome coronavirus. *Journal of Virology* **81**, 813-821 https://doi.org:doi:10.1128/JVI.02012-06 (2007).

154 Butler, Noah S. *et al.* Superior Antimalarial immunity after vaccination with late liver stage-arresting genetically attenuated parasites. *Cell Host & Microbe* **9**, 451-462 https://doi.org:10.1016/j.chom.2011.05.008 (2011).

155 Sack, B. K. *et al.* Mechanisms of stage-transcending protection following immunization of mice with late liver stage-arresting genetically attenuated malaria parasites. *PLOS Pathogens* **11**, e1004855 https://doi.org:10.1371/journal.ppat.1004855 (2015).

156 Heiss, K. *et al.* Protection from experimental cerebral malaria with a single intravenous or subcutaneous whole-parasite immunization. *Scientific Reports* **8**, 3085 https://doi.org:10.1038/s41598-018-21551-2 (2018).

157 Lewis, M. D. *et al.* Chemical attenuation of *Plasmodium* in the liver modulates severe malaria disease progression. *J Immunol* **194**, 4860-4870 https://doi.org:10.4049/jimmunol.1400863 (2015).

158 Sato, Y., Ries, S., Stenzel, W., Fillatreau, S. & Matuschewski, K. The liver-stage *Plasmodium* infection is a critical checkpoint for development of experimental cerebral malaria. *Front Immunol* **10**, 2554 https://doi.org:10.3389/fimmu.2019.02554 (2019).

159 Tjan, L. H. *et al.* Early differences in cytokine production by severity of coronavirus disease 2019. *The Journal of Infectious Diseases* **223**, 1145-1149 https://doi.org:10.1093/infdis/jiab005 (2021).

160 Kossodo, S. *et al.* Interleukin-10 modulates susceptibility in experimental cerebral malaria. *Immunology* **91**, 536-540 https://doi.org:10.1046/j.1365-2567.1997.00290.x (1997).

161 Grau, G. E. R. & Wassmer, S. C. in *Malaria: Immune Response to Infection and Vaccination* (eds Maria M. Mota & Ana Rodriguez) 67-80 (Springer International Publishing, 2017).

APPENDIX

Supplementary table 1 – List of primer sequences used for RT-qPCR analyses.

Target gene	Forward primer	Reverse primer
***P. berghei* 18S rRNA**	5'AAGCATTAAATAAAGCGAA TACATCCTTAC 3'	5' GGAGATTGGTTTTGACGT TTATGTG 3'
mouse Hprt	5' TTTGCTGACCTGCTGGATTAC 3'	5' CAAGACATTCTTTCCAGT TAAAGTTG 3'

Supplementary table 2 – Histological sample preparation protocols.

Overnight processing protocol in the Leica Tissue HistoCore Pearl	H&E staining for formalin-fixed paraffin-embedded samples
1. Tap Water for 5 min 2. 70% ethanol for 1 h 30 min 3. 70% ethanol for 1 h 30 min in vacuum 4. 96% ethanol for 1 h 30 min 5. 96% ethanol for 1 h in vacuum 6. 100% ethanol for 1 h 30 min 7. 100% ethanol for 1h 30 min in vacuum 8. Xylene for 1 h 30 min 9. Xylene for 1 h 30 min in vacuum 10. Paraffin at 70 ºC for 1 h 30 min in vacuum 11. Paraffin at 70 ºC for 1 h 30 min in vacuum	1. Depparafinization xylene 1 for 10 min 2. Depparafinization xylene 2 for 5 min 3. 100% ethanol for 5 min 4. 95% ethanol for 5 min 5. 70% ethanol for 5 min 6. Distilled water for 5 min 7. Harris Hematoxylin for 3 min 8. Running water for 5 min 9. 70% ethanol for 30 s 10. Alcoholic eosin for 10 s 11. 70% ethanol for 30 s 12. 95% ethanol for 30 s 13. 100% ethanol for 30 s 14. 100% ethanol for 30 s 15. Mounting xylene for at least 10 min 16. Mount slides

Supplementary table 3 – Lung titration medium compositions.

Homogenization medium	Dulbecco's modified Eagle's medium (DMEM, Thermo Fisher Scientific) supplemented penicillin 50 U/mL and streptomycin 50 µg/mL (Thermo Fisher Scientific)
Growth medium	Dulbecco's modified Eagle's medium (DMEM, Thermo Fisher Scientific) supplemented with 10% heat inactivated-foetal bovine serum (HI-FBS, Thermo Fisher Scientific), penicillin 50 U/mL and streptomycin 50 µg/mL (Thermo Fisher Scientific), and 2mM glutamine (Thermo Fisher Scientific)
Maintenance medium	Dulbecco's modified Eagle's medium medium (DMEM, Thermo Fisher Scientific supplemented with 2.5% heat inactivated-foetal bovine serum (HI-FBS, Thermo Fisher Scientific), penicillin 50 U/mL and streptomycin 50 µg/mL (Thermo Fisher Scientific), and 2 mM glutamine (Thermo Fisher Scientific).
Overlay medium	Maintenance medium containing 1.25% carboxymethyl cellulose (CMC, Merck)

Supplementary table 4 – Splenocyte isolation reagent compositions.

ACK lysis buffer	0.15 M NH_4Cl, 0.01 M $KHCO_3$, 0.01 M Na_2EDTA in double distilled H_20
FACS buffer	2% HI-FBS (Gibco, Thermo Fisher Scientific) in 1x PBS (Merck)

Supplementary table 5 – Composition of fluorochrome-conjugated anti-mouse monoclonal antibody mix used in the flow cytometry analysis.

Cell marker – Fluorochrome (clone)	Dilution Factor
Fixable Viability Dye (not an antibody)	1:100
CD45 – AF700 (30-F11)	1:500
B220 – Alexa Fluor 488 (RA3-6B2)	1:200
CD3 – PE-Cy7 (145-2C11)	1:100
NK1.1 – BV711 (PK136)	1:100
CD11b – PE-Cy5 (M1/70)	1:1000
Ly6C – BV605 (HK1.4)	1:200
Ly6G – PerCP-Cy5.5 (1A8)	1:200
TCR γδ – BV421 (GL3)	1:100
CD4 – APC (GK1.5)	1:100
CD8 – BV510 (53-6.7)	1:200
CD44 – BV785 (IM7)	1:100
CD62L – PE-Dazzle594 (MEL-14)	1:100

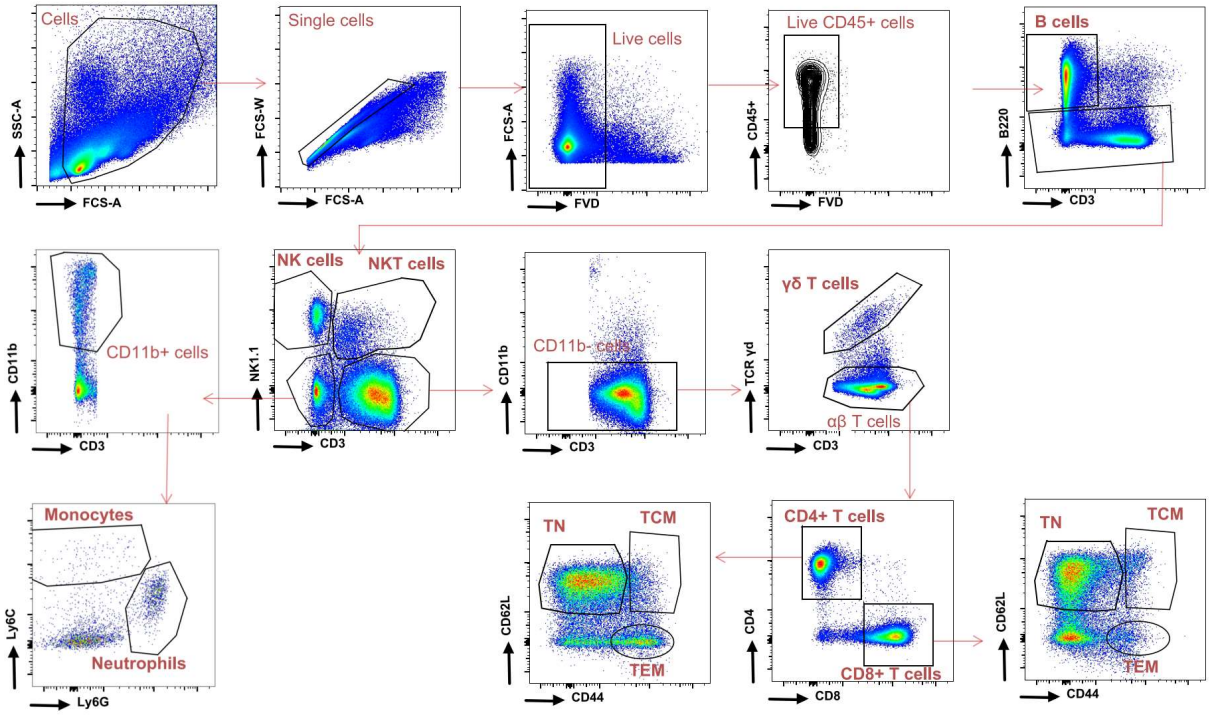

Supplementary figure 1 – Representative gating strategy employed in the identification of spleen immune populations by flow cytometry. Single cells were selected based on forward scatter (FSC) and side scatter (SSC) and dead cells were excluded using the fixable viability dye (FVD), followed by leukocyte identification by CD45 marker positivity. Immune cell populations were defined and identified resorting to the following marker staining pattern: B cells (CD3-B220+), natural killer cells (NK cells, CD3-NK1.1+), natural killer T cells (NKT cells, CD3+NK1.1+), monocytes (CD3-CD11b+Ly6C+), neutrophils (CD3-CD11b+Ly6G+), γδ T cells (CD3+CD11b-TCR γδ+), CD4 T cells (CD3+CD11b-TCR γδ-CD4+), CD8 T cells (CD3+CD11b-TCR γδ-CD8+). Subpopulations within the CD4+ T and CD8+ T cell compartments were further defined as T naïve (T_N, CD44-CD62L+), central memory (T_{CM}, CD44+CD62L+) and effector/effector memory (T_{EM}, CD44+CD62L-). SSC-A, side scatter area; FCS-A, forward scatter area; FSC-W, forward scatter width.

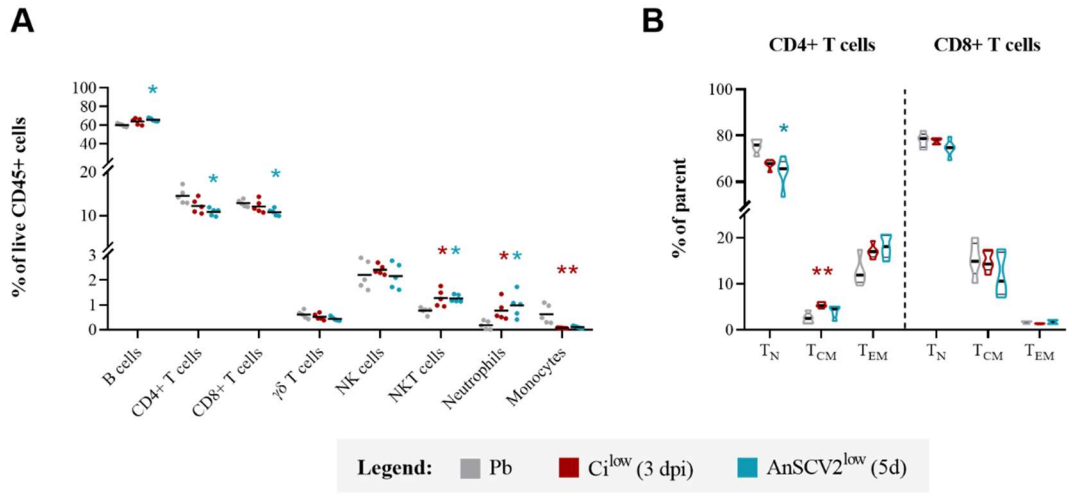

Supplementary figure 2 – **Impact of AnSCV2 and/or *P. berghei* liver infection on the main immune populations in the spleen.** Scatter dot plots for B, CD4+ T, CD8+ T, γδ T, natural killer (NK), natural killer T (NKT), neutrophil and monocyte cell population frequency within live leukocytes (CD45+), in each condition **(A)** and violin plots of the frequency of naïve (T_N), central memory (T_{CM}) or effector/effector memory (T_{EM}) populations within the CD4+ T and CD8+ T cell populations **(B)**. Experimental groups include mice infected only with *P. berghei*-single infected mice (Pb – grey symbols), mice exposed to AnSCV2^{low} infection 3 days prior to *P. berghei* inoculation (Ci^{low} (3 dpi) – red symbols) and mice only exposed to a 5-day AnSCV2^{low} infection (AnSCV2^{low} (5d) – bright blue symbols) from one experiment (n = 4-5 mice per group). The statistical significance of differences between groups was assessed by employing the Kruskal-Wallis test followed by Dunn's multiple comparisons test (* P<0.05, ** P<0.01). Coloured asterisks indicate differences relative to the overall phenotypic control group (Pb).

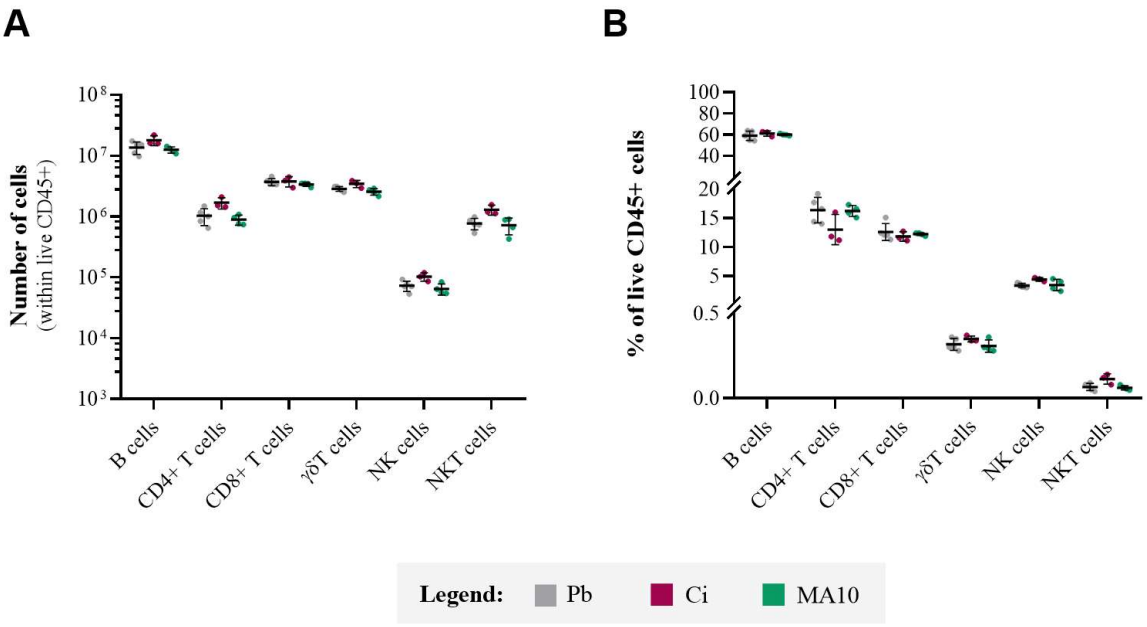

Supplementary figure 3 – Impact of MA10 and/or *P. berghei* liver infection on the main immune populations in the spleen. Scatter dot plots for B, CD4+ T, CD8+ T, γδ T, natural killer (NK) and natural killer T (NKT) cell population numbers **(A)** and frequencies **(B)** within live leukocytes (CD45+), in each condition. Experimental groups include mice only infected with *P. berghei*-single infected mice (Pb – grey symbols), mice exposed to MA10 infection 3 days prior to *P. berghei* inoculation (Ci – dark pink symbols) and mice only exposed to a 5-day MA10 infection (MA10 – green symbols) from one experiment (n = 4-5 mice per group). Statistical significance of differences between groups was assessed by employing the Kruskal-Wallis test followed by Dunn's multiple comparisons test.